$t\bar{t}b\bar{b}$ at the LHC: On the size of off-shell effects and prompt b-jet identification

G. Bevilacqua,[1] H. Y. Bi,[2] H. B. Hartanto,[3] M. Kraus,[4] M. Lupattelli,[2] and M. Worek[2]

[1]*ELKH-DE Particle Physics Research Group, University of Debrecen, H-4010 Debrecen, PBox 105, Hungary*

[2]*Institute for Theoretical Particle Physics and Cosmology, RWTH Aachen University, D-52056 Aachen, Germany*

[3]*Cavendish Laboratory, University of Cambridge, J.J. Thomson Avenue, Cambridge CB3 0HE, United Kingdom*

[4]*Physics Department, Florida State University, Tallahassee, Florida 32306-4350, USA*

(Received 16 September 2022; revised 12 December 2022; accepted 23 December 2022; published 30 January 2023)

We investigate full off-shell effects in $t\bar{t}b\bar{b}$ production in the dilepton channel at the LHC with the center-of-mass energy $\sqrt{s} = 13$ TeV. Specifically, we compute next-to-leading-order (NLO) QCD corrections to the $pp \to e^+\nu_e\mu^-\bar{\nu}_\mu b\bar{b}b\bar{b} + X$ process and provide a prescription for b-jet identification to distinguish prompt b jets from b jets originating from the decay of the top quarks. As an important irreducible background to $pp \to t\bar{t}H(H \to b\bar{b})$, $t\bar{t}$ production in association with two prompt b jets is a primary source of uncertainty in the measurement of $t\bar{t}H(H \to b\bar{b})$. In quantifying full off-shell effects, we perform comparisons between the state-of-the-art full off-shell computation and the calculation in the narrow width approximation. The former includes all double-, single- and nonresonant Feynman diagrams, interferences as well as finite-width effects of the top quarks and W gauge bosons. The latter restricts the unstable top quarks and W gauge bosons to on-shell states and includes for the first time NLO QCD corrections to both production and decays. We observe that full off-shell effects are subdominant compared to the scale uncertainties for the integrated fiducial cross section and for the majority of differential observables in the phase-space regions that we investigated. However, for a number of observables related to beyond the Standard Model searches, full off-shell effects are significant. Furthermore, with our b-jet labeling prescription, the prompt b jets and the b jets from top-quark decays can be successfully disentangled.

DOI: 10.1103/PhysRevD.107.014028

I. INTRODUCTION

The discovery of the Higgs boson at the Large Hadron Collider (LHC) [1,2] is one of the triumphs of the Standard Model (SM). The Higgs boson plays an important role in the SM since it is responsible for the electroweak (EW) symmetry breaking and the origin of the masses of the elementary particles [3–7]. The properties of the Higgs boson have been widely tested since its discovery. Until now, this particle has proven to be consistent with the expectations from the SM. The study of the coupling of the Higgs boson to the heaviest of the fundamental particles, the top quark, is crucial to test the SM and look for effects of new physics. The top-Yukawa coupling, denoted as Y_t, could be probed, for instance, via Higgs boson production in the gluon fusion process, in which the top quark appears in the loop. This $gg \to H$ channel is also sensitive to possible beyond the Standard Model (BSM) contributions, since new particles heavier than the top quark can appear in the loop. A direct probe of Y_t is provided by the Higgs boson production in association with a top-quark pair, $t\bar{t}H$ production, which was first observed at the LHC in 2018 [8,9]. Despite it being only 1% of the total Higgs boson production rate, the top-Higgs coupling is already present at tree level. The Higgs boson predominantly decays into a bottom-quark pair $H \to b\bar{b}$ with a branching ratio of $\mathcal{BR} = 58\%$ [10]. Thus, $pp \to t\bar{t}H$ with $H \to b\bar{b}$ can be measured with the best statistical precision. The measurement of $pp \to t\bar{t}H(H \to b\bar{b})$ is very challenging due to the so-called combinatorial background from the four b jets in the final state and first measurements have been reported in Ref. [11]. In addition, the QCD process $pp \to t\bar{t}b\bar{b}$ has the very same final state and represents an irreducible

background to $pp \to t\bar{t}H(H \to b\bar{b})$. The understanding of $t\bar{t}b\bar{b}$ with higher precision could help us to better isolate the Higgs boson signal from the background and, thus, improve the measurement of $t\bar{t}H(H \to b\bar{b})$ production. Moreover, $t\bar{t}b\bar{b}$ production is also important in some BSM physics studies. For instance, ATLAS and CMS experiments conduct searches for $\bar{t}bH^+(H^+ \to t\bar{b})$ [12,13], with $t\bar{t}b\bar{b}$ as a background also to this process. However, no significant excess above the expected SM background has been found so far for this process. Last but not least, $t\bar{t}b\bar{b}$ is interesting on its own as it can provide an important test of QCD and improve our understanding of the dynamics of the $g \to b\bar{b}$ splitting.

Precise predictions for $t\bar{t}b\bar{b}$ production were first computed at NLO in QCD for stable top quarks [14–18]. It was found that the NLO theoretical uncertainties stemming from the dependence on the renormalization and factorization scales are sizeable (∼33%). Furthermore, the NLO corrections are rather large (∼77%) indicating that predictions at next-to-next-to-leading-order (NNLO) QCD accuracy are needed, although such computations are not within our reach with the current technology. We note that the cross section ratio between $t\bar{t}b\bar{b}$ and $t\bar{t}jj$ processes ($\sigma_{t\bar{t}b\bar{b}}/\sigma_{t\bar{t}jj}$) has also been studied in Ref. [19]. Constructing such a ratio might help reducing the theoretical uncertainties if the two processes are correlated.[1] It was found that $t\bar{t}b\bar{b}$ and $t\bar{t}jj$ are uncorrelated due to their different jet kinematics and consequently the scale uncertainty is not significantly reduced when taking the ratio of the cross sections. To understand the origin of these large NLO corrections and gain a glimpse into the accuracy beyond NLO calculations, $t\bar{t}b\bar{b}$ production with an additional jet ($pp \to t\bar{t}b\bar{b}j + X$) has been studied in Ref. [22].

An accurate description of top-quark decays is essential to learn as much information as possible about the top-quark properties from its decay products. The inclusion of top-quark decays has been first performed through the matching of the NLO fixed-order $t\bar{t}b\bar{b}$ calculation to parton shower programs (NLO + PS) either in the 5- [23,24] or 4-flavor scheme [25,26].[2] In Ref. [26] even spin-correlated LO top-quark decays have been included. Although NLO + PS predictions allow a resummation of large logarithms via the successive soft-collinear emissions within the parton shower evolution, they account only for double-resonant top-quark contributions, meaning that the single- and nonresonant ones, which can be very important in some phase-space regions, as well as their interference effects, are omitted. Finally, for the simulations where the extra pair of b jets is only produced in the production stage of the top quarks (e.g., $t\bar{t}b\bar{b} + \mathrm{PS}$ simulations), contributions from top-quark decays with multi-bottom final states (i.e., $t \to W^+b\bar{b}b$ and $\bar{t} \to W^-\bar{b}b\bar{b}$) are only described in PS approximation. We also note that the $t\bar{t}b\bar{b}$ background to $t\bar{t}H$ also involves $t\bar{t}b\bar{b}g$ with $g \to b\bar{b}$, that can be consistently included in NLO + PS simulations of $pp \to t\bar{t}b\bar{b}$ in the 4-flavor scheme.

The inclusive fiducial cross sections of $t\bar{t}b\bar{b}$ production at the LHC and the cross section ratio $\sigma_{t\bar{t}b\bar{b}}/\sigma_{t\bar{t}jj}$ have been measured in the dilepton and lepton + jets decay channels at 8 and 13 TeV by both ATLAS and CMS experiments [28–31]. Although the theoretical predictions, provided by the NLO + PS simulations for inclusive fiducial cross sections and by the fixed-order calculation of Ref. [19] for the cross section ratio, are smaller than the measured ones, they are still compatible with the measurements within the total uncertainties.

The state-of-the-art fixed-order computation for $pp \to t\bar{t}b\bar{b}$ production in dilepton channel comprises NLO QCD corrections at $\mathcal{O}(\alpha_s^5\alpha^4)$ with full off-shell effects included. In this calculation, the top quarks and W bosons are described by Breit-Wigner propagators and all the double-, single- and nonresonant contributions (hereafter referred to as DR, SR, and NR) as well as the interference effects are consistently incorporated at the matrix element level. The full off-shell calculation for $pp \to e^+\nu_e\mu^-\bar{\nu}_\mu b\bar{b}b\bar{b} + X$ has been carried out recently by two independent groups [32,33]. In Ref. [33], the contribution of initial state bottom quarks and PDF uncertainties have been additionally investigated in detail.

In this paper, we examine the size of full off-shell effects in $t\bar{t}b\bar{b}$ production by comparing different ways of treating top-quark decays in perturbative QCD. To achieve this we employ the NLO computation performed in the narrow width approximation (NWA) with full spin correlations included. These are indeed the first predictions in the NWA fully accurate at NLO in QCD for the $pp \to e^+\nu_e\mu^-\bar{\nu}_\mu b\bar{b}b\bar{b} + X$ process. In the NWA, the top quarks and the W bosons are produced on-shell and decayed subsequently, which means that only the DR contributions are taken into account. We also provide predictions for the NWA where the NLO QCD corrections are included in the top-quark production stage but not in top-quark decays. The NWA also helps us to understand the origin of the four b jets. In this paper we work out a prescription, similar to Refs. [21,32,34,35], to distinguish the following two types of b jets:

(i) prompt b jets which are originating from $g \to b\bar{b}$ splittings,
(ii) b jets from top-quark decays, i.e., $t \to W^+b$ or $\bar{t} \to W^-\bar{b}$.

We will use our prescription to perform the labeling in the more realistic full off-shell case and compare it to the NWA.

[1] Examples where this situation occurs are the recent studies of the ratio of the correlated processes $t\bar{t}\gamma/t\bar{t}$ [20] and $t\bar{t}W^+/t\bar{t}W^-$ [21].

[2] We note that in Ref. [27] a NLO + PS computation for $t\bar{t}b\bar{b}$ production has been performed without including top-quark decays. The tool presented in that paper, however, supports automated top-quark decays with spin correlations.

The prompt b-jet identification is crucial because it enters the reconstruction of the Higgs boson in $t\bar{t}H(H \to b\bar{b})$ measurements. In that case an additional condition must be satisfied, as shown for example in Ref. [11]. Namely, the reconstructed invariant mass of the Higgs boson should be in the range of $M(bb) \in (100-140)$ GeV. In general, our prescription for the b-jet identification in $t\bar{t}b\bar{b}$ might help to improve the understanding of the signal in $t\bar{t}H(H \to b\bar{b})$ measurements.

The paper is organized as follows. In Sec. II, the theoretical setup for the LO and NLO QCD calculations is given. We then briefly review the NWA framework in Sec. III and describe our prescription to label the b jets in Sec. IV. In Sec. V we present our findings for the integrated fiducial cross sections. This is followed by the presentation of the results at a differential level in Sec. VI, with particular emphasis on full off-shell effects for a number of observables, as well as the results for b-jet labeling. Finally, in Sec. VII the results of our paper are summarized.

II. DESCRIPTION OF THE CALCULATION AND LHC SETUP

We consider the $pp \to e^+\nu_e\mu^-\bar{\nu}_\mu b\bar{b}b\bar{b} + X$ process at NLO in QCD for the LHC operating at a center-of-mass energy of $\sqrt{s} = 13$ TeV. In this paper we provide predictions for this process based on the full off-shell calculation as well as on the NWA. Both predictions have been obtained with the HELAC-NLO package [36], which is built around HELAC-PHEGAS [37]. In the HELAC-NLO framework, the phase-space integration is performed and optimized with PARNI [38] and KALEU [39]. The virtual corrections are computed with HELAC-1LOOP [40], which incorporates CutTools [41,42] and OneLoop [43] as its cornerstones. The HELAC-DIPOLES program [44] is employed to evaluate the real corrections. For the full off-shell calculation, the real corrections are computed using both Catani-Seymour [45,46] and Nagy-Soper [47] subtraction schemes. In the NWA computation the Catani-Seymour scheme is used for the subtraction of infrared divergencies in the production process, while in the case of top-quark decays, the subtraction is performed according to the scheme of Ref. [48] (see also [35] for details). In computing real emission contributions, we employ a restriction on the phase space of the dipoles, using the so-called $\alpha_{\max}$ parameter, as originally proposed for the Catani-Seymour scheme in Refs. [49,50] and for the Nagy-Soper one in Ref. [51]. The results must be independent of the choice of the $\alpha_{\max}$ parameter, and therefore, we choose two different values and check this independence. To optimize the performance of HELAC-NLO, we use reweighting techniques and MC sampling methods over the helicities and colors. The results of our full off-shell calculation are stored in the form of modified Les Houches Event Files [52] and ROOT Ntuples [53]. These event samples contain matrix-element and PDF information which allows us to reweight to different scale settings and PDF sets. Furthermore, working with event samples enables us to analyse different sets of kinematical cuts, as long as the phase-space region defined by the new set of cuts lies within the original one. Finally, also new infrared-safe observables can be produced without the need for additional time-consuming runs.

In this calculation we consider massless b quarks and work in the 5 flavor scheme. Contributions from subprocesses with b quarks in the initial states are ignored given their numerical insignificance, as shown in Ref. [33]. We keep the Cabibbo-Kobayashi-Maskawa matrix diagonal and use the same SM input parameters as in Ref. [33]

$$\begin{aligned} G_F &= 1.16638 \times 10^{-5}\ \text{GeV}^{-2}, & m_t &= 173\ \text{GeV}, \\ m_W &= 80.351972\ \text{GeV}, & \Gamma_W^{\text{NLO}} &= 2.0842989\ \text{GeV}, \\ m_Z &= 91.153481\ \text{GeV}, & \Gamma_Z^{\text{NLO}} &= 2.4942664\ \text{GeV}. \end{aligned} \tag{1}$$

As leptonic W boson decays are not subject to QCD corrections at the one-loop level, we employ the total decay widths for W and Z bosons at NLO accuracy in our calculation, i.e., for LO and NLO matrix elements. In our calculation all intermediate massive particles are consistently treated in the complex-mass scheme [54,55], where the widths of unstable particles are absorbed into the imaginary part of the corresponding mass parameters

$$\mu_i^2 = m_i^2 - i m_i \Gamma_i, \quad \text{for } i \in \{W, Z, t\}. \tag{2}$$

This choice implies a complex-valued weak mixing angle $\sin^2\theta_W = 1 - \mu_W^2/\mu_Z^2$ and guarantees gauge invariance at NLO. Complex masses are used throughout in the propagators and in all couplings, with the only exception of the electroweak coupling α. The latter is derived from the gauge-boson masses and the Fermi constant G_F in the G_μ scheme using the relation

$$\alpha = \frac{\sqrt{2}}{\pi} G_F m_W^2 \left(1 - \frac{m_W^2}{m_Z^2}\right), \tag{3}$$

namely, real masses are employed therein. Potential issues connected to the usage of a complex value of the α coupling have been discussed in the literature, see e.g., Ref. [56]. However, using complex masses instead of real ones in the derived α does not impact our predictions. We have checked explicitly that using complex masses instead of real ones in the derivation of α impacts our predictions at the level of 0.2%, i.e., it is within the MC errors. The top-quark width used for the off-shell calculation at LO, $\Gamma_{t,\text{off-shell}}^{\text{LO}}$, is computed according to Ref. [57]. The corresponding parameter for the NLO calculation, $\Gamma_{t,\text{off-shell}}^{\text{NLO}}$, is

computed by applying the procedure of Ref. [58] to the LO width. The numerical values are as follows:

$$\Gamma^{\rm LO}_{t,\rm off-shell} = 1.443303\ \text{GeV},$$
$$\Gamma^{\rm NLO}_{t,\rm off-shell} = 1.3444367445\ \text{GeV}. \tag{4}$$

A similar procedure applies in the NWA case, where in addition the following limit is taken $\Gamma_W/m_W \to 0$ as shown in Ref. [59]. In this case we get

$$\Gamma^{\rm LO}_{t,\rm NWA} = 1.466332\ \text{GeV}, \qquad \Gamma^{\rm NLO}_{t,\rm NWA} = 1.365888\ \text{GeV}. \tag{5}$$

We employ the following dynamical scale setting $\mu_R = \mu_F = \mu_0 = H_T/3$ as our central scale, where H_T is defined as

$$H_T = \sum_{i=1}^{4} p_T(b_i) + p_T(e^+) + p_T(\mu^-) + p_T^{\rm miss}, \tag{6}$$

and $p_T^{\rm miss}$ is the missing transverse momentum from the two neutrinos. For the full off-shell calculation, the theoretical uncertainty stemming from the scale dependence is obtained using the standard 7-point scale variation

$$\left(\frac{\mu_R}{\mu_0}, \frac{\mu_F}{\mu_0}\right) = \{(2,1),(0.5,1),(1,2),(1,1),(1,0.5),(2,2),(0.5,0.5)\}. \tag{7}$$

For the NWA calculation, we only use the following 3-point scale variation

$$\left(\frac{\mu_R}{\mu_0}, \frac{\mu_F}{\mu_0}\right) = \{(1,1),(2,2),(0.5,0.5)\}. \tag{8}$$

We note here that, as shown in Ref. [33], the scale variation is driven mainly by the changes in μ_R. Hence, the uncertainties will not change between the 3- and 7-point scale variations. We would like to point out that we do not vary $\alpha_s(m_t)$ entering $\Gamma_t^{\rm NLO}$ when computing the scale dependence. We checked explicitly using the NWA that such effects are small and increase the uncertainty estimates by at most 1%. We use the LHAPDF6 [60] interface and employ NNPDF3.1 [61] as the default PDF set. Specifically, we use the following two PDF sets NNPDF31_lo_as_0118 and NNPDF31_nlo_as_0118 for the LO and NLO calculation, respectively. Both PDF sets are obtained with $\alpha_s(m_Z) = 0.118$. We apply the following cuts to the charged leptons and b jets:

$$p_T(\ell) > 20\ \text{GeV}, \qquad |y(\ell)| < 2.5,$$
$$p_T(b) > 25\ \text{GeV}, \qquad |y(b)| < 2.5, \tag{9}$$

where $\ell = e^+, \mu^-$. All final-state partons with pseudorapidity $|\eta| < 5$ are recombined into jets via the anti-k_T jet algorithm [62] with $R = 0.4$, where the four-momentum recombination scheme is employed. We require exactly four b jets in the final state as well as two charged leptons. We put no restrictions on the extra light jet and $p_T^{\rm miss}$.

III. THE NARROW WIDTH APPROXIMATION

In this section we briefly review the NWA and highlight some of its features that will be exploited throughout our study. We start with the propagator of a massive unstable particle appearing in the scattering amplitude. The latter is of the form

$$\frac{1}{p^2 - m^2 + im\Gamma}, \tag{10}$$

where p, m, and Γ are the four-momentum, mass and decay width of the particle, respectively. When computing matrix elements, we deal with the squared propagator, which is given by the following Breit-Wigner distribution

$$\frac{1}{(p^2 - m^2)^2 + m^2\Gamma^2}. \tag{11}$$

In the limit $\Gamma/m \to 0$, we obtain

$$\lim_{\Gamma/m\to 0} \frac{1}{(p^2 - m^2)^2 + m^2\Gamma^2} = \frac{\pi}{m\Gamma}\delta(p^2 - m^2). \tag{12}$$

For the top quark and W gauge boson, we have with our input parameters

$$\frac{\Gamma_t}{m_t} \approx 0.008, \qquad \frac{\Gamma_W}{m_W} \approx 0.026. \tag{13}$$

The Dirac delta function in Eq. (12) enforces the on-shell production of both the top quarks and W gauge bosons. This induces a factorization of the cross section into a production and decay stage. Therefore, we can write the LO cross section in the NWA as follows:

$$\begin{aligned} d\sigma^{\rm LO}_{\rm NWA_{full}} = {} & d\sigma^{\rm LO}_{t\bar{t}b\bar{b}} \frac{d\Gamma^0_{t\to W^+b} d\Gamma^0_{\bar{t}\to W^-\bar{b}}}{(\Gamma^{\rm LO}_{t,\rm NWA})^2} \\ & + d\sigma^{\rm LO}_{t\bar{t}} \left(\frac{d\Gamma^0_{t\to W^+b\bar{b}} d\Gamma^0_{\bar{t}\to W^-\bar{b}}}{(\Gamma^{\rm LO}_{t,\rm NWA})^2} \right. \\ & \left. + \frac{d\Gamma^0_{t\to W^+b} d\Gamma^0_{\bar{t}\to W^-\bar{b}b\bar{b}}}{(\Gamma^{\rm LO}_{t,\rm NWA})^2} \right), \end{aligned} \tag{14}$$

where $d\sigma^{\rm LO}_{t\bar{t}b\bar{b}}$ ($d\sigma^{\rm LO}_{t\bar{t}}$) is the cross section of on-shell $t\bar{t}b\bar{b}$ ($t\bar{t}$) production at LO and $d\Gamma^0_{t\to W^+b}$ ($d\Gamma^0_{\bar{t}\to W^-\bar{b}}$, $d\Gamma^0_{t\to W^+b\bar{b}\bar{b}}$, $d\Gamma^0_{\bar{t}\to W^-\bar{b}b\bar{b}}$) is the differential decay rate of $t \to W^+b$ ($\bar{t} \to W^-\bar{b}$, $t \to W^+b\bar{b}$, $\bar{t} \to W^-\bar{b}b\bar{b}$) at LO. We stress

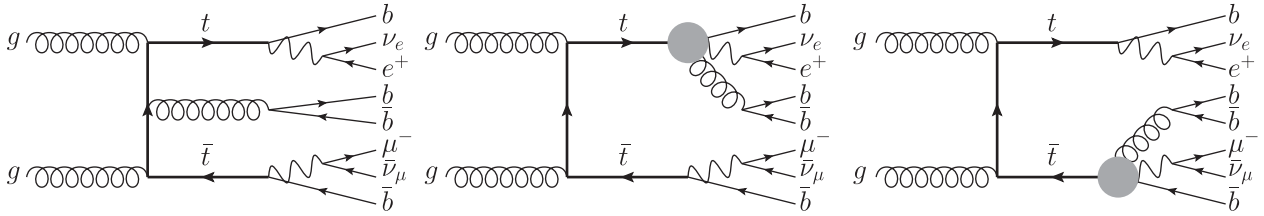

FIG. 1. Representative tree-level Feynman diagrams for the $pp \to e^+\nu_e\mu^-\bar{\nu}_\mu b\bar{b}b\bar{b}$ process in the NWA. The blob represents the $g \to b\bar{b}$ splitting in top-quark decays. The latter can be emitted either from the top quark or the bottom quark.

here that the full spin correlations are incorporated. The three terms in Eq. (14) represent the three corresponding subprocesses depicted in Fig. 1. At NLO, we can write the cross section in the NWA as follows:

$$
\begin{aligned}
d\sigma^{\rm NLO}_{\rm NWA_{full}} = {} & d\sigma^{\rm NLO}_{t\bar{t}b\bar{b}} \frac{d\Gamma^0_{t\to W^+b} d\Gamma^0_{\bar{t}\to W^-\bar{b}}}{(\Gamma^{\rm NLO}_{t,\rm NWA})^2} \\
& + d\sigma^{\rm NLO}_{t\bar{t}} \left(\frac{d\Gamma^0_{t\to W^+b\bar{b}} d\Gamma^0_{\bar{t}\to W^-\bar{b}}}{(\Gamma^{\rm NLO}_{t,\rm NWA})^2} + \frac{d\Gamma^0_{t\to W^+b} d\Gamma^0_{\bar{t}\to W^-\bar{b}b\bar{b}}}{(\Gamma^{\rm NLO}_{t,\rm NWA})^2} \right) \\
& + d\sigma^{\rm LO}_{t\bar{t}b\bar{b}} \left(\frac{d\Gamma^1_{t\to W^+b} d\Gamma^0_{\bar{t}\to W^-\bar{b}}}{(\Gamma^{\rm NLO}_{t,\rm NWA})^2} + \frac{d\Gamma^0_{t\to W^+b} d\Gamma^1_{\bar{t}\to W^-\bar{b}}}{(\Gamma^{\rm NLO}_{t,\rm NWA})^2} \right) \\
& + d\sigma^{\rm LO}_{t\bar{t}} \left(\frac{d\Gamma^1_{t\to W^+b\bar{b}} d\Gamma^0_{\bar{t}\to W^-\bar{b}}}{(\Gamma^{\rm NLO}_{t,\rm NWA})^2} + \frac{d\Gamma^1_{t\to W^+b} d\Gamma^0_{\bar{t}\to W^-\bar{b}b\bar{b}}}{(\Gamma^{\rm NLO}_{t,\rm NWA})^2} \right. \\
& \left. + \frac{d\Gamma^0_{t\to W^+b\bar{b}} d\Gamma^1_{\bar{t}\to W^-\bar{b}}}{(\Gamma^{\rm NLO}_{t,\rm NWA})^2} + \frac{d\Gamma^0_{t\to W^+b} d\Gamma^1_{\bar{t}\to W^-\bar{b}b\bar{b}}}{(\Gamma^{\rm NLO}_{t,\rm NWA})^2} \right),
\end{aligned}
\tag{15}
$$

where $d\sigma^{\rm NLO}_{t\bar{t}b\bar{b}}$ ($d\sigma^{\rm NLO}_{t\bar{t}}$) is the cross section of on-shell $t\bar{t}b\bar{b}$ ($t\bar{t}$) production at NLO and $d\Gamma^1_{t\to W^+b}$ ($d\Gamma^1_{\bar{t}\to W^-\bar{b}}$, $d\Gamma^1_{t\to W^+b\bar{b}}$, $d\Gamma^1_{\bar{t}\to W^-\bar{b}b\bar{b}}$) is the NLO correction to the differential decay rate of $t \to W^+b$ ($\bar{t} \to W^-\bar{b}$, $t \to W^+b\bar{b}$, $\bar{t} \to W^-\bar{b}b\bar{b}$). From Eq. (15) we can see that the NLO corrections can occur either in the production stage of the top quarks or in their decays. Moreover, similar to the LO calculation, prompt b jets can be produced in both stages. It is worth to point out that the various terms in Eq. (15) are separately infrared finite and do not interfere with each other.

In this work we consider predictions based on the NWA using various levels of accuracy, as described below:

(i) $\rm NWA_{full}$: all contributions in Eq. (15) are taken into account.

(ii) $\rm NWA_{LOdec}$: QCD corrections to top-quark decays are neglected. This prediction is obtained by considering only the first and second lines in Eq. (15) and using $\Gamma^{\rm LO}_{t,\rm NWA}$ in the calculation.

(iii) $\rm NWA_{prod}$: contributions where the prompt b jets originating from top-quark decays are neglected. To obtain this prediction we consider only the first and third lines in Eq. (15).

(iv) $\rm NWA_{LOdec,prod}$: both the QCD corrections to top-quark decays and the contributions of prompt b jets from top-quark decays are neglected. The contribution to this result comes from the first line of Eq. (15) only, using $\Gamma^{\rm LO}_{t,\rm NWA}$ in the calculation.

We note that the presence in Eq. (15) of the NLO top-quark width, which is a function of the strong coupling constant, spoils the rigorous expansion of the cross section in powers of α_s. As pointed out, for example in Refs. [63–68], a consistent expansion of $d\sigma^{\rm NLO}_{\rm NWA_{full}}$ in the strong coupling constant should be performed. This expansion leads to the following definition of the so-called expanded NWA cross section (further denoted by $\rm NWA_{exp}$)

$$
\begin{aligned}
d\sigma^{\rm NLO}_{\rm NWA_{exp}} = {} & d\sigma^{\rm NLO}_{\rm NWA_{full}} \left(\frac{\Gamma^{\rm NLO}_{t,\rm NWA}}{\Gamma^{\rm LO}_{t,\rm NWA}} \right)^2 \\
& - d\sigma^{\rm LO}_{\rm NWA_{full}} \frac{2(\Gamma^{\rm NLO}_{t,\rm NWA} - \Gamma^{\rm LO}_{t,\rm NWA})}{\Gamma^{\rm LO}_{t,\rm NWA}},
\end{aligned}
\tag{16}
$$

where $d\sigma^{\rm LO}_{\rm NWA_{full}}$ should be computed with $\Gamma^{\rm LO}_{t,\rm NWA}$ but employing NLO PDF sets.

Several comments are in order at this stage. The complex-mass scheme used in the full off-shell calculation is by construction gauge invariant and unitary to all orders in perturbation theory. Unitarity is violated only at fixed order due to the truncation of perturbation theory. However, the size of the violation is always a higher-order effect. Due to gauge invariance, one does not expect unnecessary

enhancements of unitarity violation [69,70]. Also in the NWA, for the dynamical scale setting ($\mu_R = \mu_F = \mu_0 = H_T/3$) there is a unitarity violation, see e.g., Ref. [67]. But, again, it is of higher orders. Generally, all three approaches (full off-shell calculation, NWA_{full} and NWA_{exp}) are a proper description of the physics of the process under consideration. They differ, of course, in the effects they contain, the full off-shell calculation being the complete one compared to the NWA results. What remains to be discussed is which version of the NWA should be compared to the full off-shell calculation in order to quantify the size of nonfactorizable corrections. In NLO QCD calculations in the NWA there are various possibilities for treating Γ_t. For example, one can set it to the numerical value corresponding to the perturbative order of the full calculation, see e.g., Ref. [65]. Alternatively, one can formally expand it according to Eq. (16). This expansion has the effect of removing systematically contributions corresponding to QCD corrections applied in both production and decays simultaneously. The latter represent formally higher-order contributions relative to the NLO QCD perturbative accuracy. We note that the size of these effects can be enhanced for processes with large NLO QCD corrections in the production part. For the $t\bar{t}b\bar{b}$ process under consideration, assuming that contributions from $g \to b\bar{b}$ splittings in top-quark decays are sufficiently small to be negligible, these effects are expected to be of the order of twice the product of the NLO QCD corrections to production and to the decay width of the top quark. Being part of the higher-order corrections to the NLO cross section, these effects should be smaller than the estimated scale uncertainties at the perturbative order considered in the calculation. For the benchmark NWA results shown in this study we will consider the results based on unexpanded top-quark width. The reason for not using this expansion for the results in the NWA should be rather clear as such a procedure can not be directly applied to the full off-shell calculations. Because the main purpose of the paper is a consistent comparison between the NWA and the full off-shell results, such approach seems to be more appropriate, see also Refs. [21,35,71–75]. However, when studying the integrated fiducial cross sections, we will also report our findings based on the expanded approach for comparison. Such a comparison will be also helpful to assess the effective impact of QCD corrections to top-quark decays in our analysis.

Finally, we would like to point out that the size of the top quark nonfactorizable corrections can be estimated directly from the full off-shell result. This can be done by rescaling the following couplings $t - W - b$ and $W - \ell - \nu_\ell$ by several large factors, as described in Refs. [59,76]. This approach should mimic the $\Gamma_t \to 0$ limit when the scattering cross section factorises into on-shell production and decay. We used both approaches, the coupling rescaling and NWA_{full}, for the simpler process, $pp \to e^+\nu_e\mu^-\bar{\nu}_\mu b\bar{b}\gamma + X$, and have shown that both methods give very similar results, see e.g., Ref. [35]. As the coupling rescaling requires the rerunning of the full off-shell calculation, we of course can not afford to do this for the more complicated $pp \to e^+\nu_e\mu^-\bar{\nu}_\mu b\bar{b}b\bar{b} + X$ process.

IV. TOP-QUARK RECONSTRUCTION AND *b*-JET IDENTIFICATION

Experimental measurements of Higgs boson properties in the $pp \to t\bar{t}H$ process with $H \to b\bar{b}$ require the identification of the Higgs boson by combining the $b\bar{b}$ pair originating from its decay. From the viewpoint of realistic analysis, the final state $t\bar{t}H \to W^+W^-b\bar{b}b\bar{b}$, where W^+W^- can decay fully leptonically ($\ell\nu_\ell\ell\nu_\ell$), semileptonically ($qq\ell\nu_\ell$) or fully hadronically ($qqqq$), consists of multiple b jets originating either from top-quark decays or the Higgs boson. The b jets which are not associated with top-quarks decays are labeled prompt b jets. However, the proper identification of prompt b jets is not free of ambiguities and can lead to substantial smearing of what would be a sharp Higgs resonance peak in the distribution of the invariant mass of the $b\bar{b}$ system. In this section we provide a prescription for labeling prompt b jets in the $pp \to e^+\nu_e\mu^-\bar{\nu}_\mu b\bar{b}b\bar{b} + X$ process. Even though we focus on the QCD $t\bar{t}b\bar{b}$ background, our conclusions can be of interest also for the case of the $pp \to t\bar{t}H(H \to b\bar{b})$ signal.

A. Full off-shell case

To perform such a labeling, in the full off-shell case we attempt to reconstruct the top quarks. The method was introduced in Ref. [77] and further discussed in e.g., Refs. [21,35]. In this paper, we generalize this method in two aspects. In Refs. [21,35], the top-quark reconstruction is based on the assumption that the charge of b and $\bar{b}$ jets can be distinguished. In our labeling procedure, first, we are going to make use of the b-jet charge information, however, we are also going to generalize this method to the case where b and $\bar{b}$ cannot be distinguished. In Refs. [21,35] the top quark is reconstructed by minimizing the function $\mathcal{Q} = |M(t) - m_t| + |M(\bar{t}) - m_t|$. In this paper, we define the function $\mathcal{Q}$ as

$$\mathcal{Q} = |M(t) - m_t| \times |M(\bar{t}) - m_t| \times |M^{\text{prompt}}(bb)|, \quad (17)$$

where $M(t)$ and $M(\bar{t})$ are the invariant mass of the candidate t and $\bar{t}$, $M^{\text{prompt}}(bb)$ is the invariant mass of the candidate pair of prompt b jets and $m_t = 173$ GeV. Compared to $\mathcal{Q} = |M(t) - m_t| + |M(\bar{t}) - m_t|$, the new definition adapts better to the actual resonant structure of the matrix elements for the process at hand. For each event, we evaluate this function for all possible resonant histories, namely all possible ways to reconstruct top-quark momenta based on the particle content of the final state. The most likely resonant history, that we take as reference to reconstruct

top quarks and thus to label prompt b jets, is the one which minimizes the function $\mathcal{Q}$. We point out that a similar prescription can be used for the identification of prompt b jets in the $pp \to t\bar{t}H(H \to b\bar{b})$ process as well. To this end it is sufficient to replace $M^{\text{prompt}}(bb)$ in Eq. (17) with $M^{\text{prompt}}(bb) - m_H$, where m_H is the Higgs boson's nominal mass of 125 GeV.

1. Charge-aware labeling

Exploiting the information of the b-jet charge, 8 resonant histories are possible at LO. Denoting the final state as $W^+W^-b_1\bar{b}_1b_2\bar{b}_2$ for ease of notation, the histories read as follows:

(1) $t \to W^+b_i$, $\bar{t} \to W^-\bar{b}_j$, $i, j = 1, 2$;
(2) $t \to W^+b_1b_2\bar{b}_1$, $\bar{t} \to W^-\bar{b}_2$, and $1 \leftrightarrow 2$;
(3) $t \to W^+b_1$, $\bar{t} \to W^-\bar{b}_1b_2\bar{b}_2$, and $1 \leftrightarrow 2$.

Here the subscripts are just used to distinguish the momenta of identical particles and do not refer to any particular ordering. We assume perfect reconstruction of the W gauge bosons, i.e., $W^+ \to e^+\nu_e$ and $W^- \to \mu^-\bar{\nu}_\mu$. In the list above, the resonant histories appearing in items 2 and 3 involve gluon emission and a subsequent splitting into a bottom-quark pair in the decay stage of the top quark and antitop quark, respectively. In this case multiple b jets enter the top-quark reconstruction, and the definition of prompt b jets as jets which are not originated from top-quark decays clearly does not apply. Nevertheless, one can still adopt a prescription to label the various b jets to be prompt or nonprompt. Let us consider, for instance, $t \to W^+b_1b_2\bar{b}_1$. We can immediately identify $\bar{b}_1$ as a prompt b jet because it can only originate from a $g \to b\bar{b}$ splitting. However in order to label b_1 and b_2, additional criteria are needed. We propose two discriminators to achieve this goal:

(1) p_T discriminator: the top-quark decay products are usually harder in p_T than those of a $g \to b\bar{b}$ splitting. Thus, we associate the b jet with the highest p_T to the top-quark decay and the other one to the prompt $b\bar{b}$ pair.
(2) ΔR discriminator: the $b\bar{b}$ pair from the gluon splitting is expected to have the smallest angular separation. Thus, the b jet that minimises $\Delta R(b_i\bar{b}_1)$ $(i = 1, 2)$ will be labeled as the prompt b jet and the remaining one will be associated to the top-quark decay.

At NLO the light jet from real radiation enters the definition of the possible resonant configurations, and 16 additional histories have to be taken into account. We note that, to mimic what is done on the experimental side, the light jet is included in the histories only when it is resolved by the jet algorithm and satisfies the following conditions: $p_T(j) > 25$ GeV and $|y(j)| < 2.5$.

2. Charge-blind labeling

If we ignore the information about the charge of the b jets, we have the following 20 histories at LO:

(1) $t \to W^+b_i$, $\bar{t} \to W^-b_j$, $i \neq j = 1, 2, 3, 4$;
(2) $t \to W^+b_1b_2b_3$, $\bar{t} \to W^-b_4$, and permutations;
(3) $t \to W^+b_1$, $\bar{t} \to W^-b_2b_3b_4$, and permutations,

where we use the symbol b for all the b and $\bar{b}$ jets. Again, the subscripts do not refer to any ordering, but are introduced to distinguish particles. In the list above, the usage of either the p_T or ΔR discriminators is relevant for the histories reported in the last two items. At NLO, there are 40 additional histories due to real radiation.

B. NWA case

The NWA allows us to assess the effectiveness of our method for labeling the b jets. Indeed we can exploit both the facts that the top quarks are always produced on-shell and that the cross section is factorized into production and decays. As a consequence of these properties, as shown in Sec. III, at LO we have three separate contributions to the cross section

(1) $pp \to t\bar{t}b\bar{b} \to (e^+\nu_e b)(\mu^-\bar{\nu}_\mu\bar{b})b\bar{b}$
(2) $pp \to t\bar{t} \to (e^+\nu_e bb\bar{b})(\mu^-\bar{\nu}_\mu\bar{b})$
(3) $pp \to t\bar{t} \to (e^+\nu_e b)(\mu^-\bar{\nu}_\mu b\bar{b}\,\bar{b})$

Therefore, we have full knowledge of the resonant history that is generated for every phase-space point. The only ambiguity left concerns contributions 2 and 3, where either the p_T or ΔR discriminator is additionally needed to label the b jets.

The labeling performed on predictions in the NWA is used as a reference for the more realistic full off-shell case. In the NWA, both the LO $M(t)$ and $M(\bar{t})$ distributions are simply given by Dirac delta distributions, however, at NLO they are smeared by extra radiation. To validate the

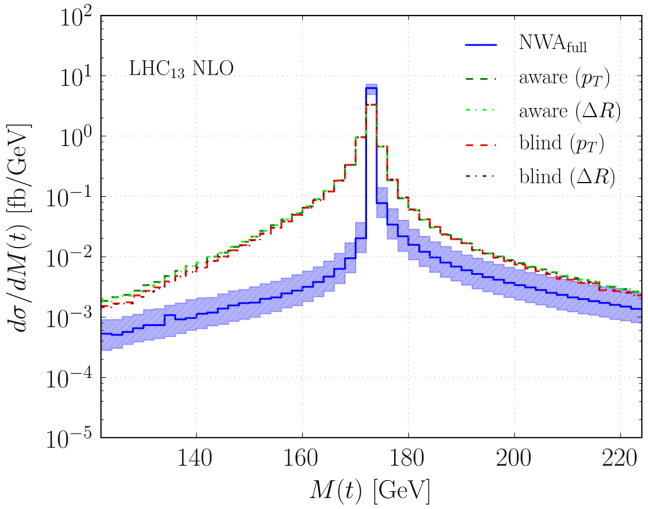

FIG. 2. Reconstructed invariant mass of the top quark at NLO in QCD for $pp \to e^+\nu_e\mu^-\bar{\nu}_\mu b\bar{b}b\bar{b} + X$ at the LHC with $\sqrt{s} = 13$ TeV. The NLO NNPDF3.1 PDF set and the dynamical scale, $\mu_R = \mu_F = \mu_0 = H_T/3$, are employed. We compare the full off-shell predictions, obtained using the charge-aware and charge-blind labeling in combination with different choices for the discriminator (p_T and ΔR), to the NWA$_{\text{full}}$ prediction.

TABLE I. Integrated fiducial cross sections at NLO in QCD for $pp \to e^+\nu_e\mu^-\bar{\nu}_\mu b\bar{b}b\bar{b} + X$ at the LHC with $\sqrt{s} = 13$ TeV. The NLO NNPDF3.1 PDF set and the dynamical scale, $\mu_R = \mu_F = \mu_0 = H_T/3$, are employed. The full off-shell prediction and its DR, SR, and NR contributions are presented along with various NWA predictions. Also given are the theoretical uncertainties coming from scale variation (δ_{scale}) and the relative differences to the NWA_{full} prediction.

Decay treatment	σ_i^{NLO} [fb]	$+\delta_{\text{scale}}$ [fb]	$-\delta_{\text{scale}}$ [fb]	$\sigma_i^{\text{NLO}}/\sigma_{\text{NWA}_{\text{full}}}^{\text{NLO}} - 1$
Off-shell	13.22 (2)	+2.65 (20%)	−2.96 (22%)	+0.5%
DR	12.08 (2)	⋯	⋯	⋯
SR	1.112 (5)	⋯	⋯	⋯
NR	0.0249 (4)	⋯	⋯	⋯
NWA_{full}	13.16 (1)	+2.61 (20%)	−2.93 (22%)	⋯
$\text{NWA}_{\text{LOdec}}$	13.22 (1)	+3.77 (29%)	−3.31 (25%)	+0.5%
NWA_{exp}	12.38 (1)	+2.91 (24%)	−2.89 (23%)	−5.9%
NWA_{prod}	13.01 (1)	+2.58 (20%)	−2.89 (22%)	−1.1%
$\text{NWA}_{\text{exp,prod}}$	12.25 (1)	+2.87 (23%)	−2.86 (23%)	−6.9%
$\text{NWA}_{\text{LOdec,prod}}$	13.11 (1)	+3.74 (29%)	−3.28 (25%)	−0.4%

top-quark reconstruction we present in Fig. 2 the $M(t)$ distribution at NLO in QCD in the vicinity of the top-quark resonance. Similar results are obtained for $M(\bar{t})$. The $M(t)$ distribution strongly peaks around the top-quark mass used in our calculation. All predictions develop a radiative tail due to final-state gluon radiation that is not recombined with the top-quark decay products. This effect is enhanced in the case of the full off-shell calculation where also finite top-quark width corrections as well as SR and NR top-quark contributions and interference effects play a crucial role.

V. INTEGRATED FIDUCIAL CROSS SECTIONS

In this section we present theoretical predictions for integrated fiducial cross sections for the $pp \to e^+\nu_e\mu^-\bar{\nu}_\mu b\bar{b}b\bar{b} + X$ process. Comparing the NWA predictions to the full off-shell results of Ref. [33] allows us to quantify the size of the full off-shell effects. Moreover, armed with our top-quark reconstruction method, we can approximately disentangle the double-, single- and non-resonant contributions in the full off-shell calculation by defining the corresponding phase-space regions, see e.g., Refs. [35,77–79]. We use the charge-aware scheme in the top-quark reconstruction and define the DR region via the following conditions:

$$|M(t) - m_t| < n\Gamma_t \quad \text{and} \quad |M(\bar{t}) - m_t| < n\Gamma_t, \tag{18}$$

where we use $n = 15$. Moreover, $M(t)$, $M(\bar{t})$ are the same quantities as those given in Eq. (17). There are two SR phase-space regions, that are given by

$$|M(t) - m_t| < n\Gamma_t \quad \text{and} \quad |M(\bar{t}) - m_t| > n\Gamma_t, \tag{19}$$

or

$$|M(t) - m_t| > n\Gamma_t \quad \text{and} \quad |M(\bar{t}) - m_t| < n\Gamma_t. \tag{20}$$

Finally, the NR region is chosen according to

$$|M(t) - m_t| > n\Gamma_t \quad \text{and} \quad |M(\bar{t}) - m_t| > n\Gamma_t. \tag{21}$$

The integrated fiducial cross sections at NLO in QCD are presented in Table I. Specifically, the full off-shell prediction and results based on the NWA at various levels of accuracy (defined in Sec. III) are presented. Comparing the full off-shell cross section with the NWA_{full} result, we found that the full off-shell effects are negligible for this process, i.e., they are below 0.5%. The theoretical uncertainties due to scale variation are of the order of 22% and are the same for both the full off-shell and the NWA_{full} calculations. Comparing the results dubbed $\text{NWA}_{\text{exp,prod}}$ and $\text{NWA}_{\text{LOdec,prod}}$ gives us an opportunity to assess the genuine impact of NLO QCD corrections to top-quark decays in the $t\bar{t}b\bar{b}$ production picture. These corrections are negative and at the level of 6.6%. On the other hand, comparing NWA_{prod} with $\text{NWA}_{\text{LOdec,prod}}$ we observed that the two results are fairly close to each other. We remark that this agreement is accidental. Indeed the NWA_{prod} cross section includes the formally suppressed higher-order contributions that have been discussed in Sec. III, which appear to be of similar size of the QCD correction to decays. We want to emphasise that the latter conclusion is, to some extent, dependent on the process under consideration and on the kinematical cuts adopted for the analysis. In addition, the theoretical uncertainty increases up to about 29% when the NLO QCD corrections to top-quark decays are omitted. By comparing the NWA_{prod} to the NWA_{full}, we found that the $t \to W^+b\bar{b}b$ and $\bar{t} \to W^-\bar{b}b\bar{b}$ contributions are at the 1.1% level. Finally, we observed that the NWA_{exp} cross section is reduced by 5.9% compared to the NWA_{full} result. Once more this effect is ascribed to the formal higher-order contributions which are present in NWA_{full}. This leads to a difference of about 6.4% between the full off-shell case and the NWA_{exp} one. The scale uncertainty for the NWA_{exp} is at the level of 24% which is still

comparable to the full off-shell case. We conclude that the various NWA predictions, as well as the full off-shell result, are in good agreement within the estimated theoretical uncertainties. Also reported in Table I are the contributions to the full off-shell cross section associated with the DR, SR, NR regions. The DR region dominates with a 91.4% contribution. It is followed by the SR region with 8.4% and finally the NR one at the level of 0.2%. Let us stress here, however, that the relative size of the various contributions depends crucially on the value of the n parameter used in the definition of those phase-space regions. To conclude this part we note that, at the integrated fiducial level, all the provided theoretical predictions for $t\bar{t}b\bar{b}$ production in dilepton channel give similar results. The differences between them are at the level of a few percent at most, thus, well within the estimated theoretical uncertainties for this process, which are of the order of 22%. Therefore, all of the predictions discussed in this section can be considered equally valid at the integrated cross-section level.

VI. DIFFERENTIAL FIDUCIAL CROSS SECTIONS

We will now present our theoretical predictions for $pp \to e^+\nu_e\mu^-\bar{\nu}_\mu b\bar{b}b\bar{b} + X$ at the differential level. We first analyse the impact of the full off-shell effects by means of systematic comparisons against the NWA. Then we perform a study of the b-jet identification in the full off-shell calculation using the $\mathrm{NWA_{full}}$ results as a benchmark to establish the validity of our approach.

A. Full off-shell effects

We have shown in Sec. V that, at the integrated fiducial level, full off-shell effects are rather small in comparison to the theoretical uncertainties originating from scale variations. This turns out to be the same for the majority of differential cross-section distributions that we have examined. By investigating a large set of observables, we found that, for most of them, we could neither detect noticeable full off-shell effects nor important contributions stemming from the corrections to top-quark decays. As an example, in Fig. 3 we show the transverse momentum distributions of the hardest and softest b jets, $p_T(b_1)$ and $p_T(b_4)$, as well as two additional observables, H_T^{vis} and H_T^{had}, defined as follows:

$$H_T^{\mathrm{had}} = \sum_{i=1}^{4} p_T(b_i), \qquad H_T^{\mathrm{vis}} = H_T^{\mathrm{had}} + \sum_{i=1}^{2} p_T(\ell_i). \quad (22)$$

Three different predictions are reported in each plot: the full off-shell, $\mathrm{NWA_{full}}$ and $\mathrm{NWA_{LOdec}}$. In the upper panel only the scale uncertainty of the full off-shell prediction is reported. The lower panel shows the ratio of the various predictions to the full off-shell one. Also given are the scale uncertainties. We can see that the three predictions are in very good agreement for the central scale values. Furthermore, the full off-shell and the $\mathrm{NWA_{full}}$ predictions have comparable theoretical uncertainties. As we observed for the case of the integrated fiducial cross section, also here the $\mathrm{NWA_{LOdec}}$ exhibits larger scale dependence.

We now turn our attention to a different set of observables, that are related to the top-quark and W-boson masses. We first introduce the minimal invariant mass of the b jet and the positron $M_{\min}(e^+b)$, defined by

$$M_{\min}(e^+b) = \min\{M(e^+b_1), M(e^+b_2), M(e^+b_3), M(e^+b_4)\}. \quad (23)$$

This observable is frequently used for top-quark mass measurements in $t\bar{t}$ production both by the ATLAS and CMS collaborations [80,81]. It is furthermore employed in various BSM analyses in the top-quark sector [82–84]. Considering the decay $t \to W^+b$, and assuming that both t and W are on-shell, the following kinematical limit applies: $M(e^+b) < \sqrt{m_t^2 - m_W^2}$. Thus, it is not surprising that the NWA at LO predicts a kinematical edge at $\sqrt{m_t^2 - m_W^2} \approx 153$ GeV in the $M_{\min}(e^+b)$ distribution. Off-shell effects at LO as well as extra-radiation effects starting from NLO are responsible for a smearing of the kinematical edge, as shown in Fig. 4.

In the next step, we study two examples of the so-called *stransverse mass*, indicated as M_{T2}, first proposed in Refs. [85,86]. To compute these observables, we adopt the algorithm of Ref. [87]. First, we study the stransverse mass of the top quark, $M_{T2}(t)$, which is defined as follows:

$$M_{T2}(t) = \min_{\sum p_T^{\nu_i} = p_T^{\mathrm{miss}}} [\max\{M_T^2(p_T(e^+X_t), p_T(\nu_1)), M_T^2(p_T(\mu^-X_{\bar{t}}), p_T(\nu_2))\}]. \quad (24)$$

The quantities $X_t, X_{\bar{t}}$ appearing in Eq. (24) indicate collectively the final-state jets associated to the decays of the $t, \bar{t}$ quarks according to the selected resonant history. Thus, at NLO, one has for example $X_t \in (b, bj, b\bar{b}, b\bar{b}j)$ and $X_{\bar{t}} \in (\bar{b}, \bar{b}j, \bar{b}b\bar{b}, \bar{b}b\bar{b}j)$. Let us note that the momenta of the two final-state neutrinos, $p(\nu_1)$ and $p(\nu_2)$, are unknown individually as they escape detection, but they satisfy the following constraint $p_T(\nu_1 + \nu_2) = p_T^{\mathrm{miss}}$. According to Eq. (24) they are defined to be the pair of momenta which minimises $M_{T2}(t)$. The quantity M_T^2 appearing in Eq. (24) is defined as follows:

$$M_T^2(p_T(\ell X), p_T(\nu)) = M^2(\ell X) + 2[E_T(\ell X)E_T(\nu) - \mathbf{p}_T(\ell X)\cdot\mathbf{p}_T(\nu)], \quad (25)$$

where $M(\ell X)$ is the invariant mass of the lepton+jet(s) system, $E_T(Y) = \sqrt{\mathbf{p}_T^2(Y) + M(Y)^2}$ and $\mathbf{p}_T = (p_x, p_y)$ is a two-component vector. Therefore, $M_T(p_T(\ell X), p_T(\nu))$ is the transverse mass of the lepton+jet(s) system for a given choice of the neutrino's momentum. It is not difficult to see

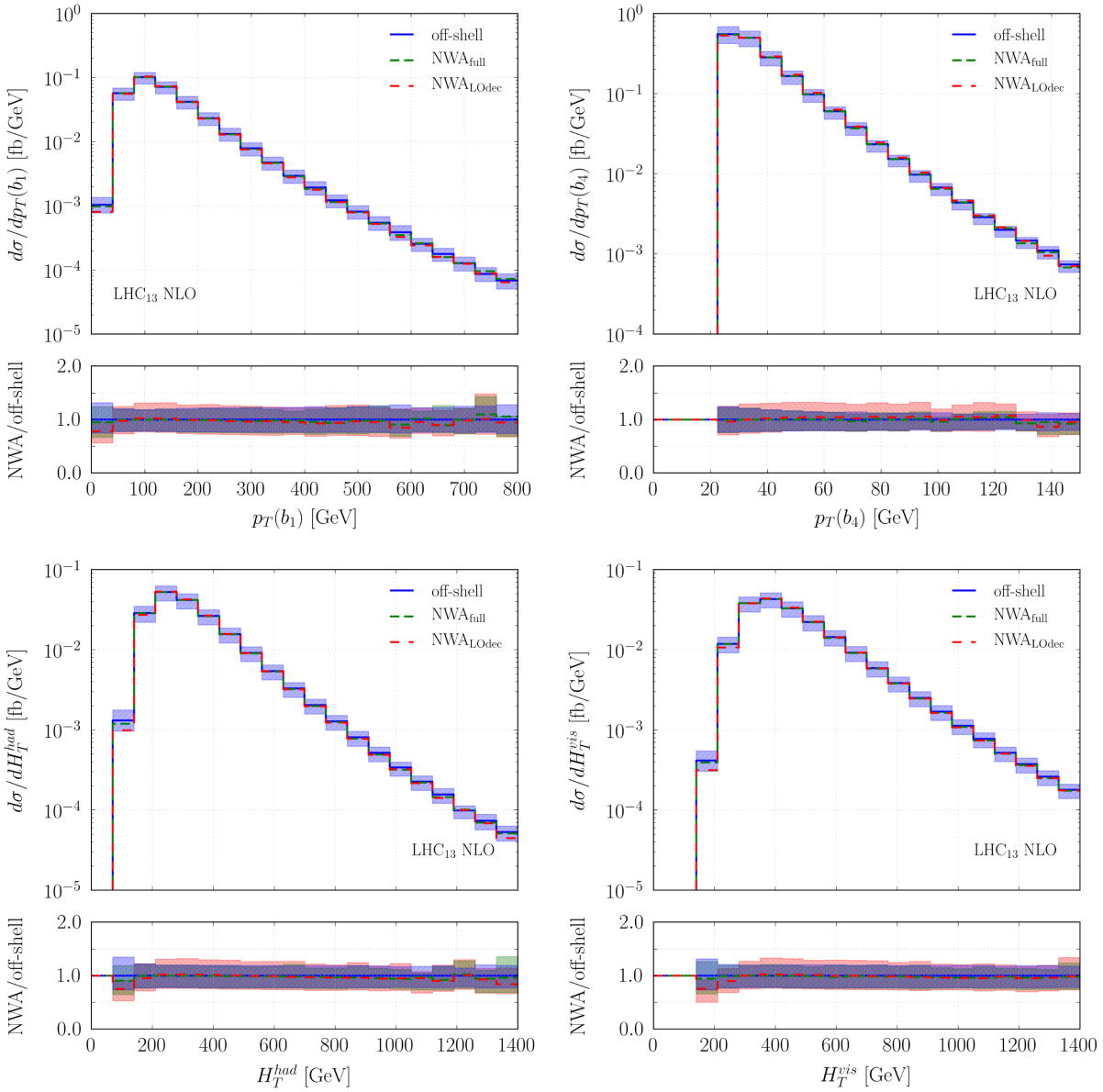

FIG. 3. Differential cross section distributions as a function of $p_T(b_1)$, $p_T(b_4)$, H_T^{had}, and H_T^{vis} at NLO in QCD for $pp \to e^+\nu_e\mu^-\bar{\nu}_\mu b\bar{b}b\bar{b} + X$ at the LHC with $\sqrt{s} = 13$ TeV. The NLO NNPDF3.1 PDF set and the dynamical scale, $\mu_R = \mu_F = \mu_0 = H_T/3$, are employed. In the upper panel, off-shell results are presented together with their scale uncertainties while only the central scale predictions are given for the NWA$_{\text{full}}$ and NWA$_{\text{LOdec}}$ case. In the lower panel, the ratios to the full off-shell calculation are shown along with the scale uncertainties.

that the $M_{T2}(t)$ observable, being expressed as a function of transverse masses according to Eq. (24), exhibits a kinematical edge at $M_{T2}(t) = m_t$. This observable is typically used in BSM searches to disentangle the possible signal of new heavy resonances from the QCD background [73,88,89]. For the NWA$_{\text{full}}$ prediction, we expect at LO an edge at m_t in the distribution of $M_{T2}(t)$. At NLO, again, the extra radiation will smear the distribution. Both LO and NLO predictions for the $M_{T2}(t)$ observable are depicted in Fig. 5.

The second M_{T2} observable we are going to discuss is the stransverse mass of the W gauge boson, $M_{T2}(W)$, defined similarly to the case of the top quark

$$M_{T2}(W) = \min_{\sum p_T^{\nu_i} = p_T^{\text{miss}}} [\max\{M_T^2(p_T(e^+), p_T(\nu_1)), M_T^2(p_T(\mu^-), p_T(\nu_2))\}], \tag{26}$$

where

$$M_T^2(p_T(\ell), p_T(\nu)) = M^2(\ell) + 2(E_T(\ell)E_T(\nu) - \mathbf{p}_T(\ell)\cdot\mathbf{p}_T(\nu)). \tag{27}$$

Also in this case, the $M_{T2}(W)$ observable has a kinematical edge but this time around m_W. For $M_{T2}(W)$ we expect a

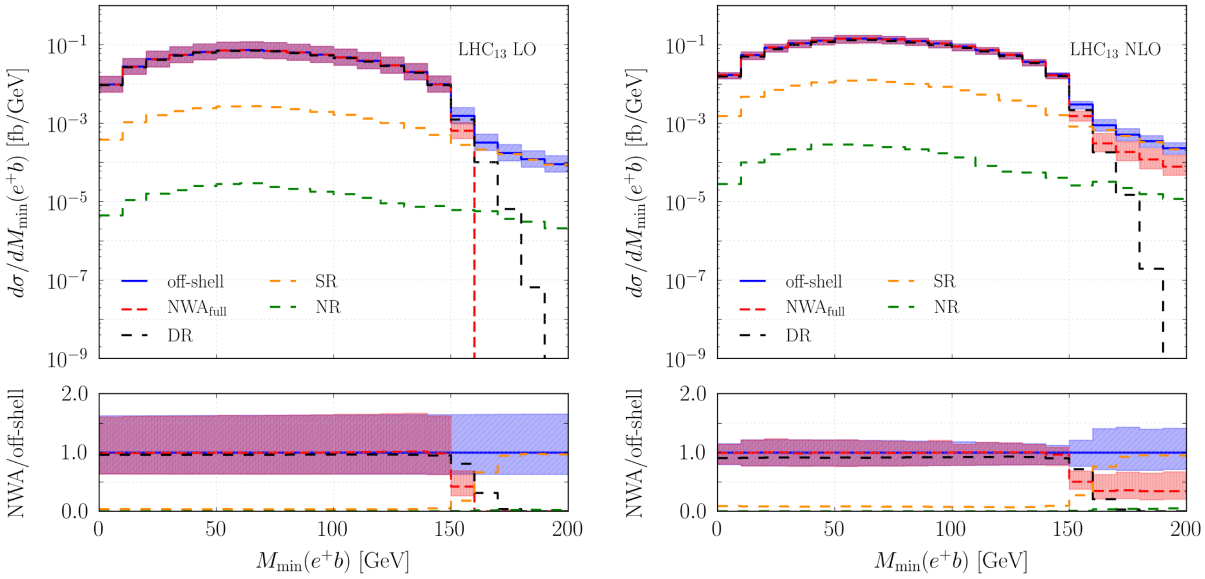

FIG. 4. Differential cross section distributions as a function of $M_{\min}(e^+b)$ at LO (left) and NLO (right) in QCD for $pp \to e^+\nu_e\mu^-\bar{\nu}_\mu b\bar{b}b\bar{b} + X$ at the LHC with $\sqrt{s} = 13$ TeV. The LO and NLO NNPDF3.1 PDF sets and the dynamical scale, $\mu_R = \mu_F = \mu_0 = H_T/3$, are employed. In the upper panel, full off-shell and NWA_{full} results are presented together with their scale uncertainties. The DR, SR, and NR contributions to the off-shell prediction are also displayed in the upper panel. In the lower panel, the ratios to the full off-shell calculation are given along with the scale uncertainties.

kinematical edge to be present at both LO and NLO accuracies, since leptonic W boson decays are not affected by QCD radiation. In Fig. 5 we also compare the predictions of the NWA_{full} to the full off-shell calculation for the $M_{T2}(W)$ observable. Uncertainty bands related to scale variation are also reported.

We note that, for all three cases considered, $M_{\min}(e^+b)$, $M_{T2}(t)$ and $M_{T2}(W)$, the NWA_{full} prediction does not adequately describe the shape of the differential cross section above the kinematical edge. The relative differences between the full off-shell case and the NWA_{full} prediction are large. Specifically, for $M_{\min}(e^+b)$ they are up to 66%, for $M_{T2}(t)$ they are of the order of 80% and for $M_{T2}(W)$ they can be as high as 90%. These differences are a consequence of the lack of single- and nonresonant contributions and interference effects as well as the of the absence of the finite top-quark and W width effects in the NWA_{full} prediction. In Figs. 4 and 5 we also report separately the DR, SR and NR contributions to the full off-shell calculation. We can see that full off-shell effects become sizeable when the SR contribution starts to dominate. For the $M_{T2}(W)$ observable, full off-shell effects come predominantly from the finite-width effects of the W boson as well as interference effects with the single W-resonant contribution. Therefore, we introduced a region decomposition similar to Eqs. (18)–(21) but applied to the W gauge boson instead of the top quarks. For this decomposition we choose $n = 5$ to accommodate the fact that the W-boson width is larger than that of the top quark.

Based on our findings, we draw the conclusion that full off-shell effects in the $t\bar{t}b\bar{b}$ process are rather small for the majority of observables used in standard analyses. We have shown, however, that in the case of observables with a kinematical edge, which are often used in BSM searches, such effects are very significant. The NWA_{full} prediction simply fails to properly describe the phase-space regions above the kinematical edge.

B. b-jet identification

Applying the techniques for b-jet identification described in Sec. IV, we can study a number of observables related to the kinematics of the b jets associated with top-quark decays as well as of those labeled as prompt b jets. We focus in particular on the invariant mass, transverse momentum and ΔR separation of the $b\bar{b}$ pairs split according to their labeling. We denote this set of observables $M^{\text{top}}(bb)$, $p_T^{\text{top}}(bb)$, $\Delta R^{\text{top}}(bb)$ and $M^{\text{prompt}}(bb)$, $p_T^{\text{prompt}}(bb)$, $\Delta R^{\text{prompt}}(bb)$ respectively. Mindful of the results presented in Sec. IV, we compare the full off-shell predictions to the NWA_{full} result taken as reference, to see how good our b-jet labeling prescription works. We report our results in Figs. 6 and 7. In the upper panel of the plots the differential cross-section distributions are reported. We also display the uncertainty band for the reference NWA_{full} case. The lower panel reports our full off-shell predictions, as obtained with different labeling approaches, normalized to the NWA_{full} prediction. We can see that the charge-aware and charge-blind labelings yield very similar predictions,

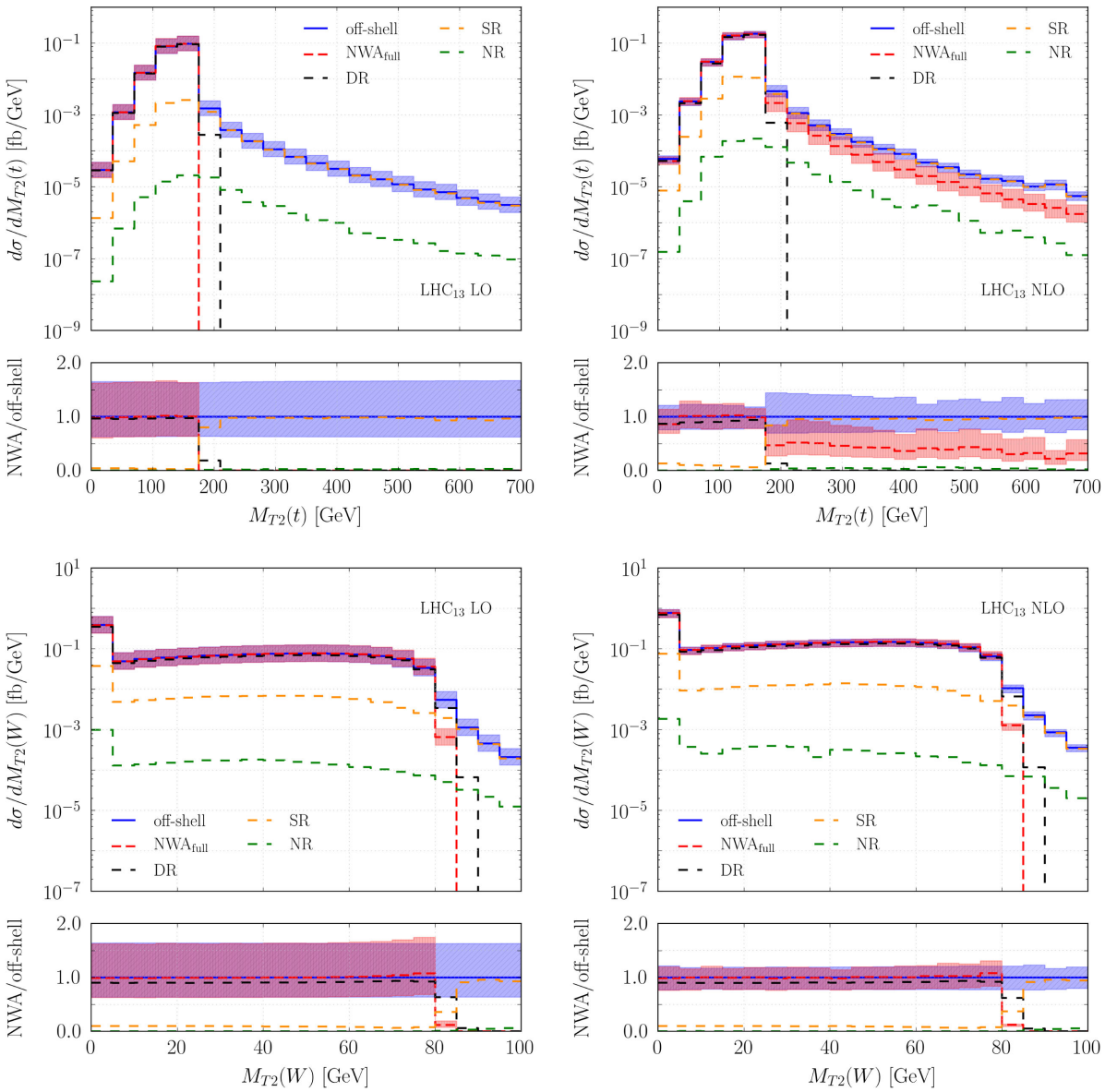

FIG. 5. Differential cross section distributions as a function of $M_{T2}(t)$ and $M_{T2}(W)$ at LO (left) and NLO (right) in QCD for $pp \to e^+\nu_e\mu^-\bar{\nu}_\mu b\bar{b}b\bar{b} + X$ at the LHC with $\sqrt{s} = 13$ TeV. The LO and NLO NNPDF3.1 PDF sets and the dynamical scale, $\mu_R = \mu_F = \mu_0 = H_T/3$, are employed. In the upper panel, full off-shell and NWA$_{\text{full}}$ results are presented together with their scale uncertainties. The DR, SR, and NR contributions to the off-shell prediction are also displayed in the upper panel. In the lower panel, the ratios to the full off-shell calculation are given along with the scale uncertainties.

which suggests that the charge information is not very crucial in our b-jet identification procedure. Moreover, we cannot see any differences between the two discriminator prescriptions. This is mainly due to the fact that the prompt b-jet pair is predominantly produced in the production stage, where the discriminator does not play any role. The predictions based on all approaches adopted for the identification of b jets are in very good agreement with the NWA$_{\text{full}}$ reference, suggesting that our labeling prescription performs very well in distinguishing between the b jets from top-quark decays and the prompt ones.

To better outline kinematical differences between $b\bar{b}$ pairs belonging to the prompt and nonprompt categories, in Fig. 8 we display afresh and in the same plot NLO differential cross-section distributions as a function of $M(bb)$, $p_T(bb)$ and $\Delta R(bb)$. We present various predictions obtained for the NWA$_{\text{full}}$ and full off-shell case. For the latter, we only report the results using the p_T discriminator. We also show the uncertainty bands as obtained from the scale dependence of the full off-shell prediction in the charge-aware case. From the $M(bb)$ distribution we can see that the spectrum of $M^{\text{prompt}}(bb)$ is softer than $M^{\text{top}}(bb)$.

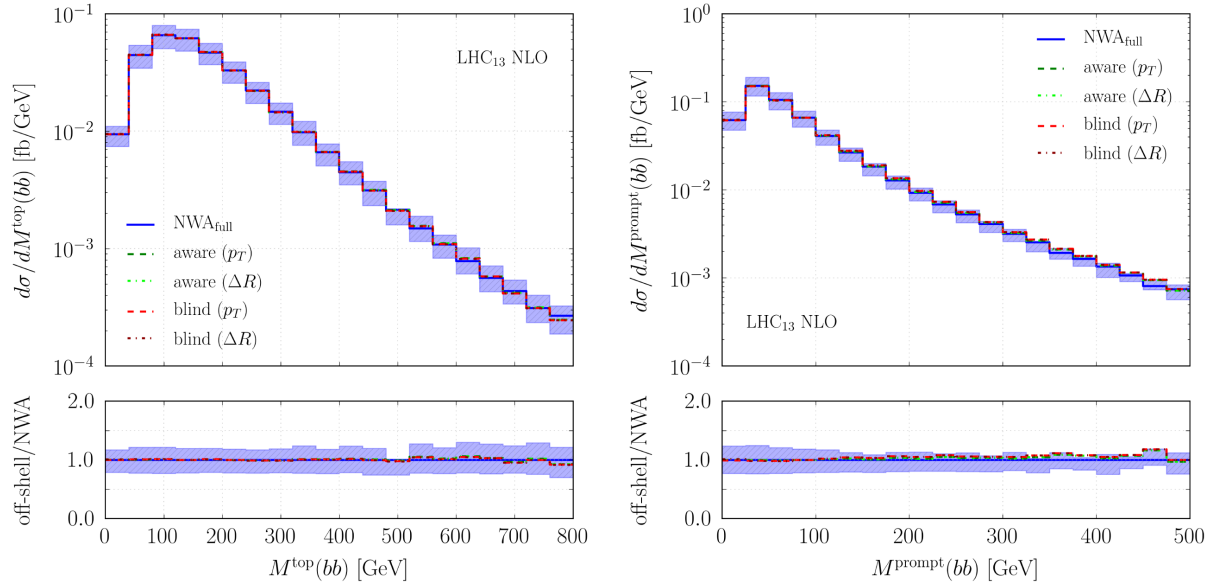

FIG. 6. Differential cross section distributions as a function of observables describing the $b\bar{b}$ pair coming from top-quark decays and the prompt $b\bar{b}$ pair at NLO in QCD for $pp \to e^+\nu_e\mu^-\bar{\nu}_\mu b\bar{b}b\bar{b} + X$ at the LHC with $\sqrt{s} = 13$ TeV. The NLO NNPDF3.1 PDF set and the dynamical scale, $\mu_R = \mu_F = \mu_0 = H_T/3$, are employed. In the upper panel, the NWA$_{\rm full}$ result is presented together with its scale uncertainty while only the central scale predictions are shown for the full off-shell predictions. The latter are obtained using the charge-aware and charge-blind labelings in combination with different choices for the discriminator (p_T and ΔR). In the lower panel, the ratios to the NWA$_{\rm full}$ calculation are given along with the scale uncertainty of the NWA$_{\rm full}$ case.

For the $p_T(bb)$ distribution we find that $p_T^{\rm top}(bb)$ decreases much faster than $p_T^{\rm prompt}(bb)$. Finally, for the $\Delta R(bb)$ distribution we can observe that the prompt b jets are more likely to have a smaller angular separation, while the b jets from top-quark decays are usually produced in back-to-back configurations. These results are consistent with expectations dictated by the dynamics of the $g \to b\bar{b}$ splitting and top-quark decays. We want to point out that one could naively think that the $b\bar{b}$ pair made of the two highest-p_T b jets is expected to originate from the $t\bar{t}$ pair. However, by comparing Fig. 8 with the corresponding plots in Ref. [33], we find that this naive prescription is not very accurate.

It is worth mentioning that several studies of the $t\bar{t}b\bar{b}$ process, that provide predictions for $M^{\rm prompt}(bb)$, $p_T^{\rm prompt}(bb)$ and $\Delta R^{\rm prompt}(bb)$ distributions at NLO QCD accuracy, are available in the literature. In the first studies of this kind, see e.g., Refs. [16,17,19,90], top quarks were treated as stable particles, which makes the identification of prompt b jets straightforward. We can use these results as important benchmarks to assess the performance of our b-jet labeling prescription. The issue of b-jet identification in the $t\bar{t}b\bar{b}$ process has also been studied more recently using deep neural network techniques, see e.g., Refs. [91–93]. The results presented in this section are fully consistent with the findings from earlier studies mentioned above. Very good agreement is found in the shape of the distributions as well as in the location of the peaks. This confirms even further that our simple b-jet labeling prescription works very well.

VII. SUMMARY

In this paper we investigated the impact of the full off-shell effects in the $pp \to e^+\nu_e\mu^-\bar{\nu}_\mu b\bar{b}b\bar{b} + X$ process at NLO in QCD by presenting a comprehensive comparison between the full off-shell calculation and the NWA predictions. This is the first time that the full NWA predictions at NLO in QCD, including higher-order corrections to both production and decay stages as well as NLO spin correlations, have been presented for the $t\bar{t}b\bar{b}$ process in the dilepton channel. Let us stress that dropping the approximation of on-shell top quarks and W gauge bosons in the calculation of the $e^+\nu_e\mu^-\bar{\nu}_\mu b\bar{b}b\bar{b} + X$ final state not only increases dramatically the complexity of the calculation but also represents a qualitatively different level of theoretical description.

At the integrated fiducial level, we found that the full off-shell effects are very small, of the order of 0.5%, which is compatible with the expected size $\mathcal{O}(\Gamma_t/m_t)$. Moreover, the scale uncertainties for both the NWA$_{\rm full}$ and the full off-shell calculation are the same and at the level of 22%. We observed that the NLO QCD corrections to top-quark decays are negative and amount to 6.6%. We also observed that the scale uncertainty is slightly larger if top-quark decays are treated with LO accuracy. Indeed, it increases up to 29%. Additionally, we noticed that the contribution of

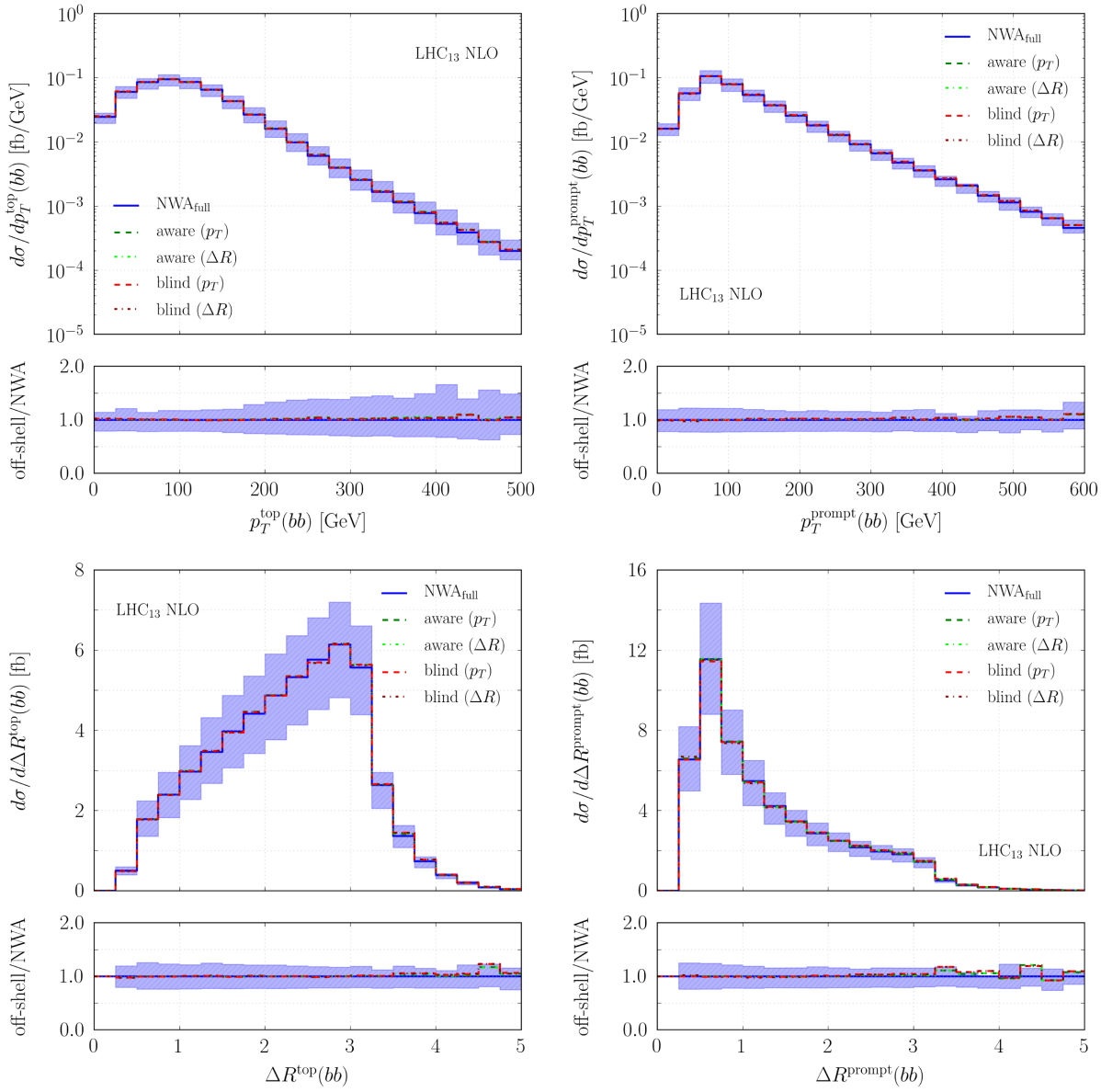

FIG. 7. Differential cross section distributions as a function of observables describing the $b\bar{b}$ pair coming from top-quark decays and the prompt $b\bar{b}$ pair at NLO in QCD for $pp \to e^+\nu_e\mu^-\bar{\nu}_\mu b\bar{b}b\bar{b} + X$ at the LHC with $\sqrt{s} = 13$ TeV. The NLO NNPDF3.1 PDF set and the dynamical scale, $\mu_R = \mu_F = \mu_0 = H_T/3$, are employed. In the upper panel, the NWA_{full} result is presented together with its scale uncertainty while only the central scale predictions are shown for the full off-shell predictions. The latter are obtained using the charge-aware and charge-blind labelings in combination with different choices for the discriminator (p_T and ΔR). In the lower panel, the ratios to the NWA_{full} calculation are given along with the scale uncertainty of the NWA_{full} case.

prompt b jets originating from top-quark decays is only of the order of 1% in the setup of our analysis. At the differential level, for a large number of observables, the full off-shell effects are small for the energy ranges we considered. Not only the NWA_{full} prediction agrees very well with the full off-shell result, but also the theoretical uncertainties due to missing higher-order corrections are very similar. The scale uncertainty bands for the $\text{NWA}_{\text{LOdec}}$ case, however, are generally larger. Nevertheless, all predictions are in good agreement within the corresponding theoretical uncertainties. Our findings suggest that NWA_{full} is a good approximation for the $pp \to e^+\nu_e\mu^-\bar{\nu}_\mu b\bar{b}b\bar{b} + X$ process for a large number of observables. However, substantial full off-shell effects are present for observables with kinematic edges. These effects originate from single- and nonresonant contributions, interference effects as well as from top-quarks and W-bosons finite-width corrections.

In this paper we also provided a prescription to distinguish prompt b jets from b jets that come from top-quark decays. The importance of this study is related to the fact

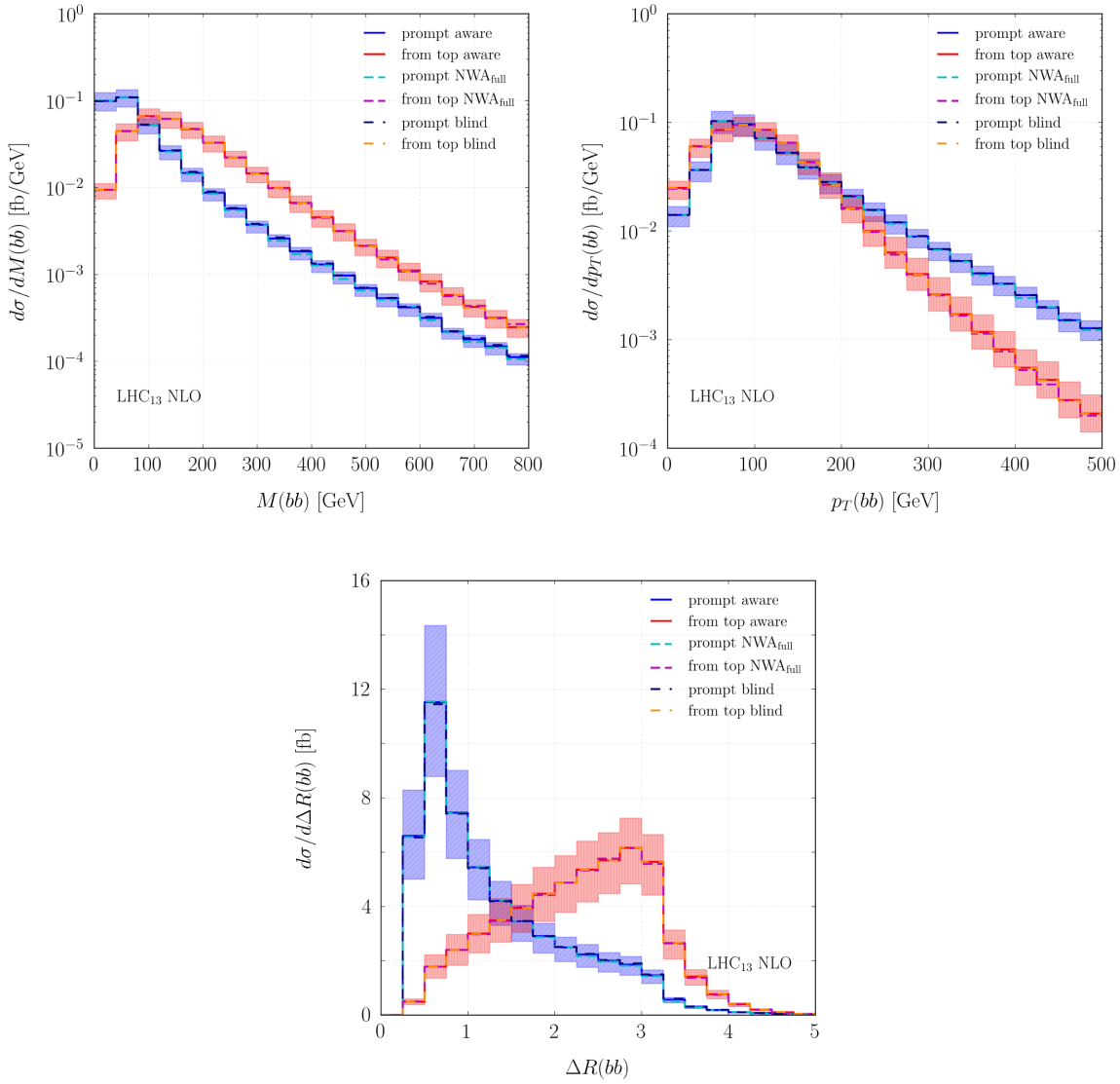

FIG. 8. Differential cross section distributions as a function of observables describing the $b\bar{b}$ pair coming from top-quark decays and the prompt $b\bar{b}$ pair at NLO in QCD for $pp \to e^+\nu_e\mu^-\bar{\nu}_\mu b\bar{b}b\bar{b} + X$ at the LHC with $\sqrt{s} = 13$ TeV. The NLO NNPDF3.1 PDF set and the dynamical scale, $\mu_R = \mu_F = \mu_0 = H_T/3$, are employed. The distributions for the two $b\bar{b}$ pairs are reported in the same plot. The NWA$_{\text{full}}$ results are presented together with the full off-shell predictions, which are obtained using the charge-aware and charge-blind labelings with the p_T discriminator. The scale uncertainty bands for the charge-aware predictions are also displayed.

that the $pp \to t\bar{t}b\bar{b}$ process has the same final state as $pp \to t\bar{t}H$ production when the Higgs boson decays into $H \to b\bar{b}$. This particular decay chain is crucial for the direct measurement of the top-quark-Higgs and bottom-quark-Higgs Yukawa couplings. Complementary to the widely used deep neural network approaches adopted in the literature, we proposed a kinematic-based prescription where we looked for the most likely resonant history which might have generated the corresponding final state. We applied our prescription to the full off-shell calculation using the NWA results as a benchmark. By studying the $M(bb)$, $p_T(bb)$ and $\Delta R(bb)$ distributions of the b jets we found that our prescription is able to capture the different origin of the b jets which appear in the final state.

ACKNOWLEDGMENTS

The work of H. Y. B., M. L., and M. W. was supported by the Deutsche Forschungsgemeinschaft (DFG) under the following Grants No. 396021762—TRR 257: *P3H—Particle Physics Phenomenology after the Higgs Discovery* and No. 400140256—GRK 2497: *The physics of the heaviest particles at the LHC*. Support by a grant of the Bundesministerium für Bildung und Forschung (BMBF) is additionally acknowledged. The research of G. B. is supported by Grant No. K 125105 of the National Research, Development and Innovation Office in Hungary. H. B. H. has received funding from the European Research Council (ERC) under the European Union's Horizon 2020 Research and

Innovation Programme (Grant Agreement No. 683211). Furthermore, the work of H. B. H has been partially supported by STFC consolidated HEP theory Grant No. ST/T000694/1. The work of M. K. was supported in part by the U.S. Department of Energy under Grant No. DE-SC0010102. Simulations were performed with computing resources granted by RWTH Aachen University under Projects No. `rwth0414`, No. `rwth0878`, and No. `rwth0846`.

[1] G. Aad *et al.* (ATLAS Collaboration), Observation of a new particle in the search for the Standard Model Higgs boson with the ATLAS detector at the LHC, Phys. Lett. B **716**, 1 (2012).
[2] S. Chatrchyan *et al.* (CMS Collaboration), Observation of a new boson at a mass of 125 GeV with the CMS experiment at the LHC, Phys. Lett. B **716**, 30 (2012).
[3] S. L. Glashow, Partial symmetries of weak interactions, Nucl. Phys. **22**, 579 (1961).
[4] S. Weinberg, A Model of Leptons, Phys. Rev. Lett. **19**, 1264 (1967).
[5] A. Salam, Weak and electromagnetic interactions, Conf. Proc. C **680519**, 367 (1968).
[6] P. W. Higgs, Broken Symmetries and the Masses of Gauge Bosons, Phys. Rev. Lett. **13**, 508 (1964).
[7] F. Englert and R. Brout, Broken Symmetry and the Mass of Gauge Vector Mesons, Phys. Rev. Lett. **13**, 321 (1964).
[8] M. Aaboud *et al.* (ATLAS Collaboration), Observation of Higgs boson production in association with a top quark pair at the LHC with the ATLAS detector, Phys. Lett. B **784**, 173 (2018).
[9] A. M. Sirunyan *et al.* (CMS Collaboration), Observation of $t\bar{t}H$ Production, Phys. Rev. Lett. **120**, 231801 (2018).
[10] G. Aad *et al.* (ATLAS and CMS Collaborations), Measurements of the Higgs boson production and decay rates and constraints on its couplings from a combined ATLAS and CMS analysis of the LHC pp collision data at $\sqrt{s} = 7$ and 8 TeV, J. High Energy Phys. 08 (2016) 045.
[11] G. Aad *et al.* (ATLAS Collaboration), Measurement of Higgs boson decay into b-quarks in associated production with a top-quark pair in pp collisions at $\sqrt{s} = 13$ TeV with the ATLAS detector, J. High Energy Phys. 06 (2022) 097.
[12] G. Aad *et al.* (ATLAS Collaboration), Search for charged Higgs bosons decaying into a top quark and a bottom quark at $\sqrt{s} = 13$ TeV with the ATLAS detector, J. High Energy Phys. 06 (2021) 145.
[13] A. M. Sirunyan *et al.* (CMS Collaboration), Search for a charged Higgs boson decaying into top and bottom quarks in events with electrons or muons in proton-proton collisions at $\sqrt{s} = 13$ TeV, J. High Energy Phys. 01 (2020) 096.
[14] A. Bredenstein, A. Denner, S. Dittmaier, and S. Pozzorini, NLO QCD corrections to $t\bar{t}b\bar{b}$ production at the LHC: 1. Quark-antiquark annihilation, J. High Energy Phys. 08 (2008) 108.
[15] A. Bredenstein, A. Denner, S. Dittmaier, and S. Pozzorini, NLO QCD Corrections to $pp \to t\bar{t}b\bar{b} + X$ at the LHC, Phys. Rev. Lett. **103**, 012002 (2009).
[16] G. Bevilacqua, M. Czakon, C. G. Papadopoulos, R. Pittau, and M. Worek, Assault on the NLO wishlist: $pp \to t\bar{t}b\bar{b}$, J. High Energy Phys. 09 (2009) 109.
[17] A. Bredenstein, A. Denner, S. Dittmaier, and S. Pozzorini, NLO QCD corrections to top anti-top bottom anti-bottom production at the LHC: 2. Full hadronic results, J. High Energy Phys. 03 (2010) 021.
[18] M. Worek, On the next-to-leading order QCD K-factor for top $t\bar{t}b\bar{b}$ production at the TeVatron, J. High Energy Phys. 02 (2012) 043.
[19] G. Bevilacqua and M. Worek, On the ratio of $t\bar{t}b\bar{b}$ and $t\bar{t}jj$ cross sections at the CERN Large Hadron Collider, J. High Energy Phys. 07 (2014) 135.
[20] G. Bevilacqua, H. B. Hartanto, M. Kraus, T. Weber, and M. Worek, Precise predictions for $t\bar{t}\gamma/t\bar{t}$ cross section ratios at the LHC, J. High Energy Phys. 01 (2019) 188.
[21] G. Bevilacqua, H.-Y. Bi, H. B. Hartanto, M. Kraus, J. Nasufi, and M. Worek, NLO QCD corrections to off-shell $t\bar{t}W^{\pm}$ production at the LHC: Correlations and asymmetries, Eur. Phys. J. C **81**, 675 (2021).
[22] F. Buccioni, S. Kallweit, S. Pozzorini, and M. F. Zoller, NLO QCD predictions for $t\bar{t}b\bar{b}$ production in association with a light jet at the LHC, J. High Energy Phys. 12 (2019) 015.
[23] A. Kardos and Z. Trócsányi, Hadroproduction of t anti-t pair with a b anti-b pair using PowHel, J. Phys. G **41**, 075005 (2014).
[24] M. V. Garzelli, A. Kardos, and Z. Trócsányi, Hadroproduction of $t\bar{t}b\bar{b}$ final states at LHC: Predictions at NLO accuracy matched with parton shower, J. High Energy Phys. 03 (2015) 083.
[25] G. Bevilacqua, M. V. Garzelli, and A. Kardos, $t\bar{t}b\bar{b}$ hadroproduction with massive bottom quarks with PowHel, arXiv:1709.06915.
[26] T. Ježo, J. M. Lindert, N. Moretti, and S. Pozzorini, New NLOPS predictions for $t\bar{t} + b$-jet production at the LHC, Eur. Phys. J. C **78**, 502 (2018).
[27] F. Cascioli, P. Maierhöfer, N. Moretti, S. Pozzorini, and F. Siegert, NLO matching for $t\bar{t}b\bar{b}$ production with massive b-quarks, Phys. Lett. B **734**, 210 (2014).
[28] CMS Collaboration, Measurement of the cross section ratio $t\bar{t}b\bar{b}/t\bar{t}jj$ in pp collisions at 8 TeV, CERN Technical Report No. CMS-PAS-TOP-13-010, 2013.
[29] M. Aaboud *et al.* (ATLAS Collaboration), Measurements of inclusive and differential fiducial cross-sections of $t\bar{t}$ production with additional heavy-flavour jets in proton-proton collisions at $\sqrt{s} = 13$ TeV with the ATLAS detector, J. High Energy Phys. 04 (2019) 046.

[30] A. M. Sirunyan *et al.* (CMS Collaboration), Measurements of $t\bar{t}$ cross sections in association with b jets and inclusive jets and their ratio using dilepton final states in pp collisions at $\sqrt{s} = 13$ TeV, Phys. Lett. B **776**, 355 (2018).

[31] A. M. Sirunyan *et al.* (CMS Collaboration), Measurement of the cross section for $\mathrm{t\bar{t}}$ production with additional jets and b jets in pp collisions at $\sqrt{s} = 13$ TeV, J. High Energy Phys. 07 (2020) 125.

[32] A. Denner, J.-N. Lang, and M. Pellen, Full NLO QCD corrections to off-shell $t\bar{t}b\bar{b}$ production, Phys. Rev. D **104**, 056018 (2021).

[33] G. Bevilacqua, H.-Y. Bi, H. B. Hartanto, M. Kraus, M. Lupattelli, and M. Worek, $t\bar{t}b\bar{b}$ at the LHC: On the size of corrections and b-jet definitions, J. High Energy Phys. 08 (2021) 008.

[34] A. Denner, R. Feger, and A. Scharf, Irreducible background and interference effects for Higgs-boson production in association with a top-quark pair, J. High Energy Phys. 04 (2015) 008.

[35] G. Bevilacqua, H. B. Hartanto, M. Kraus, T. Weber, and M. Worek, Off-shell vs on-shell modelling of top quarks in photon associated production, J. High Energy Phys. 03 (2020) 154.

[36] G. Bevilacqua, M. Czakon, M. V. Garzelli, A. van Hameren, A. Kardos, C. G. Papadopoulos, R. Pittau, and M. Worek, HELAC-NLO, Comput. Phys. Commun. **184**, 986 (2013).

[37] A. Cafarella, C. G. Papadopoulos, and M. Worek, HELAC-PHEGAS: A generator for all parton level processes, Comput. Phys. Commun. **180**, 1941 (2009).

[38] A. van Hameren, PARNI for importance sampling and density estimation, Acta Phys. Pol. B **40**, 259 (2009).

[39] A. van Hameren, KALEU: A general-purpose parton-level phase space generator, arXiv:1003.4953.

[40] A. van Hameren, C. G. Papadopoulos, and R. Pittau, Automated one-loop calculations: A proof of concept, J. High Energy Phys. 09 (2009) 106.

[41] G. Ossola, C. G. Papadopoulos, and R. Pittau, Reducing full one-loop amplitudes to scalar integrals at the integrand level, Nucl. Phys. **B763**, 147 (2007).

[42] G. Ossola, C. G. Papadopoulos, and R. Pittau, CutTools: A program implementing the OPP reduction method to compute one-loop amplitudes, J. High Energy Phys. 03 (2008) 042.

[43] A. van Hameren, OneLoop: For the evaluation of one-loop scalar functions, Comput. Phys. Commun. **182**, 2427 (2011).

[44] M. Czakon, C. G. Papadopoulos, and M. Worek, Polarizing the dipoles, J. High Energy Phys. 08 (2009) 085.

[45] S. Catani and M. H. Seymour, A general algorithm for calculating jet cross-sections in NLO QCD, Nucl. Phys. **B485**, 291 (1997); Erratum, Nucl. Phys. **B510**, 503 (1998).

[46] S. Catani, S. Dittmaier, M. H. Seymour, and Z. Trocsanyi, The dipole formalism for next-to-leading order QCD calculations with massive partons, Nucl. Phys. **B627**, 189 (2002).

[47] G. Bevilacqua, M. Czakon, M. Kubocz, and M. Worek, Complete Nagy-Soper subtraction for next-to-leading order calculations in QCD, J. High Energy Phys. 10 (2013) 204.

[48] J. M. Campbell, R. K. Ellis, and F. Tramontano, Single top production and decay at next-to-leading order, Phys. Rev. D **70**, 094012 (2004).

[49] Z. Nagy and Z. Trocsanyi, Next-to-leading order calculation of four jet observables in electron positron annihilation, Phys. Rev. D **59**, 014020 (1998).

[50] Z. Nagy, Next-to-leading order calculation of three jet observables in hadron hadron collision, Phys. Rev. D **68**, 094002 (2003).

[51] M. Czakon, H. B. Hartanto, M. Kraus, and M. Worek, Matching the Nagy-Soper parton shower at next-to-leading order, J. High Energy Phys. 06 (2015) 033.

[52] J. Alwall *et al.*, A standard format for Les Houches event files, Comput. Phys. Commun. **176**, 300 (2007).

[53] I. Antcheva *et al.*, ROOT: A C++ framework for petabyte data storage, statistical analysis and visualization, Comput. Phys. Commun. **180**, 2499 (2009).

[54] A. Denner, S. Dittmaier, M. Roth, and D. Wackeroth, Predictions for all processes $e^+e^- + 4$ fermions $+\gamma$, Nucl. Phys. **B560**, 33 (1999).

[55] A. Denner, S. Dittmaier, M. Roth, and L. H. Wieders, Electroweak corrections to charged-current $e^+e^- \to 4$ fermion processes: Technical details and further results, Nucl. Phys. **B724**, 247 (2005); Erratum, Nucl. Phys. **B854**, 504 (2012).

[56] R. Frederix, S. Frixione, V. Hirschi, D. Pagani, H. S. Shao, and M. Zaro, The automation of next-to-leading order electroweak calculations, J. High Energy Phys. 07 (2018) 185; Erratum, J. High Energy Phys. 11 (2021) 85.

[57] M. Jeżabek and J. H. Kühn, QCD corrections to semileptonic decays of heavy quarks, Nucl. Phys. **B314**, 1 (1989).

[58] L. Basso, S. Dittmaier, A. Huss, and L. Oggero, Techniques for the treatment of IR divergences in decay processes at NLO and application to the top-quark decay, Eur. Phys. J. C **76**, 56 (2016).

[59] A. Denner, S. Dittmaier, S. Kallweit, and S. Pozzorini, NLO QCD corrections to off-shell top-antitop production with leptonic decays at hadron colliders, J. High Energy Phys. 10 (2012) 110.

[60] A. Buckley, J. Ferrando, S. Lloyd, K. Nordström, B. Page, M. Rüfenacht, M. Schönherr, and G. Watt, LHAPDF6: Parton density access in the LHC precision era, Eur. Phys. J. C **75**, 132 (2015).

[61] R. D. Ball *et al.* (NNPDF Collaboration), Parton distributions from high-precision collider data, Eur. Phys. J. C **77**, 663 (2017).

[62] M. Cacciari, G. P. Salam, and G. Soyez, The anti-k_t jet clustering algorithm, J. High Energy Phys. 04 (2008) 063.

[63] K. Melnikov and M. Schulze, NLO QCD corrections to top quark pair production and decay at hadron colliders, J. High Energy Phys. 08 (2009) 049.

[64] K. Melnikov, M. Schulze, and A. Scharf, QCD corrections to top quark pair production in association with a photon at hadron colliders, Phys. Rev. D **83**, 074013 (2011).

[65] K. Melnikov, A. Scharf, and M. Schulze, Top quark pair production in association with a jet: QCD corrections and jet radiation in top quark decays, Phys. Rev. D **85**, 054002 (2012).

[66] A. Behring, M. Czakon, A. Mitov, A. S. Papanastasiou, and R. Poncelet, Higher Order Corrections to Spin Correlations in Top Quark Pair Production at the LHC, Phys. Rev. Lett. **123**, 082001 (2019).

[67] M. Czakon, A. Mitov, and R. Poncelet, NNLO QCD corrections to leptonic observables in top-quark pair production and decay, J. High Energy Phys. 05 (2021) 212.

[68] J. Campbell and K. Ellis, Top-quark processes at NLO in production and decay, J. Phys. G **42**, 015005 (2015).

[69] A. Denner and J. N. Lang, The complex-mass scheme and unitarity in perturbative quantum field theory, Eur. Phys. J. C **75**, 377 (2015).

[70] A. Denner and S. Dittmaier, The complex-mass scheme for perturbative calculations with unstable particles, Nucl. Phys. B, Proc. Suppl. **160**, 22 (2006).

[71] J. Alcaraz Maestre *et al.* (SM, NLO MULTILEG Working Group, SM MC Working Group), The SM and NLO multileg and SM MC working groups: Summary report, in *Proceedings of the 7th Les Houches Workshop on Physics at TeV Colliders* (2012), pp. 1–220, arXiv:1203.6803.

[72] G. Bevilacqua, H.-Y. Bi, H. B. Hartanto, M. Kraus, and M. Worek, The simplest of them all: $t\bar{t}W^{\pm}$ at NLO accuracy in QCD, J. High Energy Phys. 08 (2020) 043.

[73] J. Hermann and M. Worek, The impact of top-quark modelling on the exclusion limits in $t\bar{t}+\mathrm{DM}$ searches at the LHC, Eur. Phys. J. C **81**, 1029 (2021).

[74] G. Bevilacqua, H. Y. Bi, F. Febres Cordero, H. B. Hartanto, M. Kraus, J. Nasufi, L. Reina, and M. Worek, Modeling uncertainties of $t\bar{t}W^{\pm}$ multilepton signatures, Phys. Rev. D **105**, 014018 (2022).

[75] D. Stremmer and M. Worek, Production and decay of the Higgs boson in association with top quarks, J. High Energy Phys. 02 (2022) 196.

[76] G. Bevilacqua, M. Czakon, A. van Hameren, C. G. Papadopoulos, and M. Worek, Complete off-shell effects in top quark pair hadroproduction with leptonic decay at next-to-leading order, J. High Energy Phys. 02 (2011) 083.

[77] N. Kauer and D. Zeppenfeld, Finite width effects in top quark production at hadron colliders, Phys. Rev. D **65**, 014021 (2002).

[78] S. Liebler, G. Moortgat-Pick, and A. S. Papanastasiou, Probing the top-quark width through ratios of resonance contributions of $e^+e^- \to W^+W^-b\bar{b}$, J. High Energy Phys. 03 (2016) 099.

[79] A. Baskakov, E. Boos, and L. Dudko, Model independent top quark width measurement using a combination of resonant and nonresonant cross sections, Phys. Rev. D **98**, 116011 (2018).

[80] M. Aaboud *et al.* (ATLAS Collaboration), Measurement of the top quark mass in the $t\bar{t} \to$ dilepton channel from $\sqrt{s} = 8$ TeV ATLAS data, Phys. Lett. B **761**, 350 (2016).

[81] A. M. Sirunyan *et al.* (CMS Collaboration), Measurement of the top quark mass in the dileptonic $t\bar{t}$ decay channel using the mass observables $M_{b\ell}$, M_{T2}, and $M_{b\ell\nu}$ in pp collisions at $\sqrt{s} = 8$ TeV, Phys. Rev. D **96**, 032002 (2017).

[82] U. Haisch and G. Polesello, Searching for heavy Higgs bosons in the $t\bar{t}Z$ and tbW final states, J. High Energy Phys. 09 (2018) 151.

[83] U. Haisch and G. Polesello, Searching for production of dark matter in association with top quarks at the LHC, J. High Energy Phys. 02 (2019) 029.

[84] A. M. Sirunyan *et al.* (CMS Collaboration), Search for pair production of first-generation scalar leptoquarks at $\sqrt{s} = 13$ TeV, Phys. Rev. D **99**, 052002 (2019).

[85] C. G. Lester and D. J. Summers, Measuring masses of semiinvisibly decaying particles pair produced at hadron colliders, Phys. Lett. B **463**, 99 (1999).

[86] A. Barr, C. Lester, and P. Stephens, A variable for measuring masses at hadron colliders when missing energy is expected; m(T2): The truth behind the glamour, J. Phys. G **29**, 2343 (2003).

[87] C. G. Lester and B. Nachman, Bisection-based asymmetric M_{T2} computation: A higher precision calculator than existing symmetric methods, J. High Energy Phys. 03 (2015) 100.

[88] G. Aad *et al.* (ATLAS Collaboration), Search for direct top-squark pair production in final states with two leptons in pp collisions at $\sqrt{s} = 8$ TeV with the ATLAS detector, J. High Energy Phys. 06 (2014) 124.

[89] U. Haisch, P. Pani, and G. Polesello, Determining the *CP* nature of spin-0 mediators in associated production of dark matter and $t\bar{t}$ pairs, J. High Energy Phys. 02 (2017) 131.

[90] D. de Florian *et al.* (LHC Higgs Cross Section Working Group Collaboration), Handbook of LHC Higgs cross sections: 4. Deciphering the nature of the Higgs sector, CERN Yellow Report: Monograph (2017), Vol. **2**, arXiv:1610.07922.

[91] J. Choi, T. J. Kim, J. Lim, J. Park, Y. Ryou, J. Song, and S. Yun, Identification of additional jets in the $t\bar{t}b\bar{b}$ events by using deep neural network, J. Korean Phys. Soc. **77**, 1100 (2020).

[92] C. Jang, S.-K. Ko, Y.-K. Noh, J. Choi, J. Lim, and T. J. Kim, Learning to increase matching efficiency in identifying additional b-jets in the $t\bar{t}b\bar{b}$ process, Eur. Phys. J. Plus **137**, 870 (2022).

[93] L. Cavallini, A. Coccaro, C. K. Khosa, G. Manco, S. Marzani, F. Parodi, D. Rebuzzi, A. Rescia, and G. Stagnitto, Tagging the Higgs boson decay to bottom quarks with colour-sensitive observables and the Lund jet plane, Eur. Phys. J. C **82**, 493 (2022).